The Human Respiratory Syncytial Virus Nonstructural Protein 1 Regulates Type I and Type II Interferon Pathways*[S]

Marcus L. Hastie‡, Madeleine J. Headlam‡, Nirav B. Patel‡§, Alexander A. Bukreyev¶‖, Ursula J. Buchholz¶, Keyur A. Dave‡, Emma L. Norris‡, Cassandra L. Wright‡, Kirsten M. Spann, Peter L. Collins¶, and Jeffrey J. Gorman‡ ‡‡**

Respiratory syncytial viruses encode a nonstructural protein (NS1) that interferes with type I and III interferon and other antiviral responses. Proteomic studies were conducted on human A549 type II alveolar epithelial cells and type I interferon-deficient Vero cells (African green monkey kidney cells) infected with wild-type and NS1-deficient clones of human respiratory syncytial virus to identify other potential pathway and molecular targets of NS1 interference. These analyses included two-dimensional differential gel electrophoresis and quantitative Western blotting. Surprisingly, NS1 was found to suppress the induction of manganese superoxide dismutase (SOD2) expression in A549 cells and to a much lesser degree Vero cells in response to infection. Because SOD2 is not directly inducible by type I interferons, it served as a marker to probe the impact of NS1 on signaling of other cytokines known to induce SOD2 expression and/or indirect effects of type I interferon signaling. Deductive analysis of results obtained from cell infection and cytokine stimulation studies indicated that interferon-γ signaling was a potential target of NS1, possibly as a result of modulation of STAT1 levels. However, this was not sufficient to explain the magnitude of the impact of NS1 on SOD2 induction in A549 cells. Vero cell infection experiments indicated that NS1 targeted a component of the type I interferon response that does not directly induce SOD2 expression but is required to induce another initiator of SOD2 expression. STAT2 was ruled out as a target of NS1 interference using quantitative Western blot analysis of infected A549 cells, but data were obtained to indicate that STAT1 was one of a number of potential targets of NS1. A label-free mass spectrometry-based quantitative approach is proposed as a means of more definitive identification of NS1 targets. ***Molecular & Cellular Proteomics 11: 10.1074/mcp.M111.015909, 108–127, 2012.***

Human respiratory syncytial virus (hRSV)[1] is the most important cause of lower respiratory tract disease in infants and young children and can also cause serious disease in immunocompromised adults and the elderly (1–5). Bronchiolitis and pneumonia caused by hRSV are associated with substantial morbidity and occasional mortality. It is estimated that most children are infected with hRSV at least once by 2 years of age (2–4), and infection of very young infants is controversially linked to a predisposition to asthma later in life (6, 7). The global annual RSV infection rate is estimated to be 64 million, resulting in ~160,000 deaths (World Health Organization Initiative for Vaccine Research, 2010). Early attempts to control hRSV with a formalin-inactivated vaccine resulted in poor protection and enhanced hRSV disease when previously hRSV-naïve vaccine recipients experienced subsequent natural infection (2, 8–10). Despite substantial efforts over the years, no hRSV vaccine has been licensed (1, 2, 4, 10). The only pharmaceutical agent currently used to treat established RSV infections, ribavirin, is inconvenient, expensive, has toxicity risks and is only of modest efficacy (1, 2). Monoclonal antibodies are used prophylactically, but this is expensive, inconvenient, and restricted to use with high risk individuals (10, 11). Accordingly, a number of studies are underway to

From the ‡Protein Discovery Centre, Queensland Institute of Medical Research, Herston, Queensland 4029, Australia, the ¶Respiratory Virus Section, Laboratory of Infectious Diseases, NIAID, National Institutes of Health, Bethesda, Maryland 20892, and the **University of Queensland, Clinical Medical Virology Centre, and The Royal Children's Hospital, Sir Albert Sakzewski Virus Research Centre, Herston, Queensland 4029, Australia

⌘ *Author's Choice*—Final version full access.

Received November 15, 2011, and in revised form, January 23, 2012

Published, MCP Papers in Press, February 9, 2012, DOI 10.1074/mcp.M111.015909

[1] The abbreviations used are: hRSV, human respiratory syncytial virus; DIGE, differential gel electrophoresis; AKR1B1, aldose reductase; APOL2, apolipoprotein L2; CAT, catalase; CapHPLC, capillaryHPLC; GFP, green fluorescent protein; IFN, interferon; IFIT3, interferon-induced protein with tetratricopeptide repeats 3; ISG, interferon stimulated gene; LTQ, linear trap quadrupole; MS/MS, tandem mass spectrometry; NRF2, nuclear factor erythroid 2-related factor 2; SOD2, mitochondrial Mn superoxide dismutase 2; STAT, signal transducer and activator of transcription; TBS, 10 mM Tris-HCl (pH 7.4) containing 0.15 M NaCl; TBST, TBS containing 0.5% (v/v) Tween 20; TXNRD1, thioredoxin reductase 1, cytosolic; WARS, tryptophanyl-tRNA synthetase; E-values, expected values; ANOVA, analysis of variance.

redress the unmet need for vaccines and pharmaceuticals for hRSV (10, 12–14).

Human RSV belongs to the *Pneumovirus* genus of the *Paramyxoviridae* family of lipid membrane-encapsidated, single-strand, negative sense RNA viruses (1–3). The hRSV genome of 15.2 kb encodes 10 subgenomic mRNAs, from which 11 proteins are translated (1–3). Like other members of the *Paramyxoviridae*, these proteins function in viral attachment and fusion, viral replication, and evasion of the host immune defenses (1–3). Live recombinant wild-type and mutant hRSVs have been produced from cDNA by reverse genetics (15–20). These recombinant hRSVs have greatly facilitated vaccine development studies (21–24). Recombinant manipulation of hRSV has also allowed assessment of the contribution of hRSV-encoded proteins to virus replication (16–20, 25–27) and host cell responses (3, 20, 28–36). NS1 and NS2 (nonstructural proteins 1 and 2 of respiratory syncytial virus) are relatively small hRSV encoded proteins that are not packaged with mature virions but act within the infected cell to suppress host cell type I and type III interferon (IFN) induction and signaling (29–37) and other antiviral responses (28, 32). Other members of the *Paramyxoviridae* produce IFN antagonist proteins that are generally derived from genes that encode other proteins (38); however, hRSV NS1 and NS2 are encoded by discrete viral genes (1–3, 39). Thus, it has been possible to produce live recombinant hRSVs with the genes encoding NS1 and/or NS2 deleted. These recombinant hRSVs have provided substantial insight into the broad impact of these proteins on host cell innate antiviral responses (16, 17, 19, 20, 25, 27–36). Despite this, the structures and mechanisms of action of NS1 and NS2 are incompletely characterized at the molecular level. The present study was initiated to assess the impact of NS1 on hRSV infection of human A549 type II alveolar epithelial cells at the proteomic level as a way of identifying potential molecular targets of NS1 interference. This is the first study involving proteomic analysis of cells infected with hRSV with a gene deleted from the viral genome.

Using two-dimensional differential gel electrophoresis (DIGE), we observed that relatively few A549 cellular proteins were regulated upon infection with wild-type recombinant hRSV expressing the green fluorescent protein (GFP) from an inserted gene (WT-GFP hRSV, a recombinant clone of human respiratory syncytial virus containing the wild-type A2 subtype genome expressing the green fluorescent protein from an inserted gene). A greater number of proteins were regulated in A549 cells infected with a clone of hRSV, from which the NS1 gene was deleted (ΔNS1-GFP hRSV, a recombinant clone of human respiratory syncytial virus containing the wild-type A2 subtype genome with the NS1 sequence deleted and expressing the green fluorescent protein from an inserted gene), even though viral gene expression by this mutant was reduced compared with WT-GFP hRSV. Most of these regulated cellular proteins were identified as the products of IFN-stimulated genes (ISGs). However, there was also a substantial induction of manganese superoxide dismutase (SOD2) expression in cells infected with ΔNS1-GFP hRSV in addition to the previously documented up-regulation of SOD2 by WT-GFP hRSV (40). The induction of SOD2 was demonstrated using two-dimensional DIGE, label-free mass spectrometry, Western blotting, and quantitative real time PCR. Measurement of SOD2 in uninfected A549 cells exposed to various cytokines indicated that regulation of SOD2 by NS1 in hRSV-infected A549 cells was potentially via an impact on IFN-γ signaling. Further experiments were conducted with infected IFN-deficient Vero cells and cytokine-stimulated Vero cells to facilitate identification of pathway and molecular targets of NS1. Although it was confirmed that type I IFNs do not directly induce SOD2, it was evident that a type I ISG was required for SOD2 induction in response to infection. The previously purported susceptibility of STAT2 to NS1-promoted proteosomal degradation (37) was not supported by the present findings, but other potential targets of NS1 are discussed together with experimental approaches to identify these targets.

EXPERIMENTAL PROCEDURES

Materials—General biochemical reagents were obtained from Sigma-Aldrich. Acids and organic solvents were HPLC grade or better. All of the materials and reagents for two-dimensional DIGE were obtained from GE Healthcare. This included 24-cm nonlinear pH 3–11 IPG DryStrips, IPG strip covering fluid, nonlinear pH 3–11 IPG buffer, cyanine dye labeling reagents, and kits for protein enrichment and quantitation.

Primary antibodies included a mouse monoclonal antibody to SOD2, a mouse polyclonal antiserum to interferon-induced protein with tetratricopeptide repeats 3 (IFIT3) obtained from Abcam (Cambridge, UK), rabbit polyclonal antisera to STAT1 and thioredoxin reductase 1 (TXNRD1) from Cell Signaling Technology (Beverly, MA), rabbit polyclonal antisera to STAT2 and nuclear factor erythroid 2-related factor 2 (NRF2) from Santa Cruz (Santa Cruz, CA), a rabbit polyclonal antiserum to catalase (CAT) from Merck, and a goat polyclonal antiserum to hRSV obtained from Virostat (Westbrook, ME). Anti-rabbit IgG IR680LT, anti-mouse, and anti-goat IgG IRDye 800CW secondary antibodies were purchased from LI-COR (Lincoln, NE). SyproRuby® was obtained from Invitrogen.

Trypsin (modified sequencing grade) was purchased from Roche Diagnostics. α-Cyano-4-hydroxy cinnamic acid was from Bruker Daltonics (Bremen, Germany). Water was purified using a Milli-Q Synthesis system (Millipore, Billerica, MA). Denaturants for in-solution IEF fractionation of proteins were purchased in OFFGEL kit form (catalogue number 5188-6424) from Agilent Technologies. All of the components of the denaturing buffer (pH 7.6) used for cell lysis were obtained from Thermo Fisher Scientific (Rockford, IL). This buffer comprised 25 mM Tris-HCl, 150 mM NaCl, 1% (v/v) Nonidet P-40, 1% (w/v) sodium deoxycholate, 0.1% (w/v) SDS, phosphatase inhibitors (Halt phosphatase inhibitor mixture of sodium fluoride, sodium orthovanadate, sodium pyrophosphate, and β-glycerophosphate), and protease inhibitors (Halt protease inhibitor mixture of 1 mM 4-(2-aminoethyl) benzenesulfonyl fluoride hydrochloride, 0.8 μM aprotinin, 50 μM bestatin, 15 μM E-64, 5 μM EDTA, and 20 μM leupeptin). Opti-MEM cell culture medium was purchased from Invitrogen, and FCS was from HyClone (Logan, UT).

IFN-α and -β were from PBL Medical Laboratories (Piscataway, NJ), and IFN-λ1 (interleukin-29) was from PeproTech (Rock Hill, NJ). TNF-α was from Prospec-Tany Technogene (Israel). Interleukin-1β (IL-1β) and IFN-γ were from R & D Systems (MN). All of the cytokines were produced by recombinant expression of human genes. The functional activities of the IFNs were confirmed by demonstrating their abilities to induce IFN signaling, as indicated by translocation of STAT2 from the cytoplasm to the nuclei of treated cells (41).

Cell Culture, Virus Infection, and Lysate Preparation—The recombinant viruses used in this study were a variant of the WT A2 strain of hRSV that expressed GFP from an inserted gene (WT-GFP hRSV) or this GFP construct lacking the NS1 protein (ΔNS1-GFP hRSV) prepared as described previously (20). Approximately 10 million A549 or African green monkey Vero cells were infected at a multiplicity of infection of 3 plaque-forming units/cell with the viruses above or exposed to medium only (mock infected) in Opti-MEM® medium supplemented with 2.5% (v/v) FCS and 50 μg/ml gentamycin (Quality Biologicals, Gaithersburg, MD). The cells were cultured for a further 24 h, at which time the medium was removed, and the cells were washed twice with ice-cold phosphate-buffered saline. 1 ml of the ice-cold denaturing lysis buffer mixture described above was added directly to the flasks containing the washed cells. The flasks were then kept on ice for 5 min and subsequently scraped, and the resultant lysates were transferred to microcentrifuge tubes. The lysates were clarified by centrifugation at 14,000 $\times$ *g* and 4 °C for 15 min. The supernatants were transferred into clean tubes and stored frozen at −80 °C prior to transfer by air freight (World Courier) from the National Institutes of Health (Bethesda, MD) to Brisbane, Australia, in the constant presence of dry ice.

Cytokine Induction—A549 or Vero cells were cultured in Opti-MEM® medium supplemented with 10% (v/v) FCS, 100 μg/ml streptomycin, and 100 units/ml penicillin. Approximately 10 million cells were treated with complete medium (20 ml) containing either 0.1% (w/v) BSA or cytokine in 0.1% (w/v) BSA. The cells were then incubated at 37 °C for 24 h before being washed twice, lysed, and clarified by centrifugation as described above.

Protein Enrichment, Quantitation and Cyanine Dye Labeling—Lysates were individually enriched for proteins using a two-dimensional clean-up kit (GE Healthcare) according to the manufacturer's instructions. The protein pellets resulting from 24-h cultures of ~10 million infected or IFN-stimulated cells were resuspended in 60–80 μl of 30 mM Tris-HCl buffer (pH 8.8) containing 7 M urea, 2 M thiourea, and 4% (w/v) CHAPS and used immediately or stored at −80 °C until required. A protein assay (GE Healthcare 2D Quant Kit) was used to estimate protein concentrations following the manufacturer's instructions. Typically 1.5 mg of protein was recovered per lysate.

Individual samples were minimally labeled with *N*-hydroxysuccinimidyl ester derivatives of the charge matched Cy3 or Cy5 dyes developed specifically for two-dimensional DIGE (GE Healthcare) according to the manufacturer's instructions. Briefly, 50 μg of each enriched protein sample in 10 μl of labeling buffer (30 mM Tris-HCl, 7 M urea, 2 M thiourea, 4% (w/v) CHAPS, pH 8.8) was labeled with 400 pmol of either Cy3- or Cy5-reactive dyes, freshly dissolved in 1 μl of anhydrous dimethyl formamide. The labeling reaction was incubated at 0 °C in the dark for 30 min, and the reaction was terminated by addition of 10 nmol of lysine (1 μl of 10 mM) and incubated at 0 °C for a further 10 min. Internal controls containing equal quantities of all samples for a particular experiment (total of 50 μg) were prepared by reaction in the same way with the equivalent Cy2Dye.

Two-dimensional Electrophoresis—50 μg of Cy3- and Cy5-labeled samples were pooled, and 50 μg of Cy2-labeled internal control sample was added for quantitative two-dimensional DIGE analysis. Alternatively, 400–700 μg of enriched, but unlabeled lysate proteins were separated on two-dimensional gels using essentially identical protocols. IPG strips were rehydrated for 15 h at 22 °C in 450 μl of rehydration buffer containing 7 M urea, 2 M thiourea, 4% (w/v) CHAPS, 0.002% (w/v) bromphenol blue, 40 mM DTT, 0.5% (v/v) pH 3–11 NL IPG buffer, and the relevant samples using an Ettan IPGphor reswelling tray (GE Healthcare). Once rehydration was complete, the samples were focused at 20 °C using Ettan™ IPGphor 3 (GE Healthcare) system at 500 V for 500 Vh, followed by a gradient to 1 kV over 800 Vh, a gradient to 10 kV over 16.5 kVh, and maintained at 10 kV for another 22.2 kVh (total 40 kVh). The strips were either used immediately after focusing or stored at −80 °C for later processing. The strips were thawed at 22 °C if required and incubated in equilibration buffer containing 6 M urea, 30% (v/v) glycerol, 2% (w/v) SDS, 50 mM Tris-HCl (pH 8.8), 1% (w/v) DTT for 15 min on a rocker at 22 °C. The strips were then equilibrated for an additional 15 min in the buffer above but with 2.5% (w/v) iodoacetamide instead of DTT. The equilibrated strips were sealed onto the top of 1-mm-thick 12% discontinuous (42) polyacrylamide slab gels (26 $\times$ 20 cm) with 0.5% (w/v) agarose sealing solution. For two-dimensional DIGE analysis, these slab gels were polymerized between low fluorescence glass plates. Standard glass plates were used for preparative gels, with one plate precoated with bind silane (GE Healthcare). Second dimension separations were performed on an Ettan DALT six electrophoresis unit (GE Healthcare). The proteins were separated at 25 °C, initially with 1 W (8 mA)/gel for 1.5 h, followed by 13 W (40 mA)/gel until the dye front approached the bottom of the gels.

Image Scanning and Analysis of Two-dimensional DIGE Gels—Two-dimensional DIGE gels were scanned directly between low fluorescence glass plates using a Fujifilm FLA-9000 laser scanner (excitation/emission, Cy2 473 nm/510 nm LP, Cy3 532 nm/570 nm df20, Cy5 635 nm/665 nm LP) at 100-μm resolution. The images were then trimmed using Multigauge software 3.0 (Fuji Photo Film Co. Ltd.) and data sets analyzed in Delta2D 4.1 (Decodon GmbH). The gels were aligned using the internal control and the Delta2D in-gel warping strategy followed by fusion of all gels and spot detection on this fused image. The coordinates defining all spots were then transferred to individual gels to attain 100% spot alignment between gels. The resulting intensities were analyzed in the TIGR multiple experiment viewer incorporated into Delta2D using the Welch *t* test (*p* values based on all permutations of the data) applying the standard Bonferroni correction. Spots that exhibited a fold change of at least 1.2 and a significance threshold of $\alpha < 0.01$ were selected for further analysis.

Falsely colored gel images were constructed using the protein patterns originating from the Cy3- and Cy5-labeled samples. For this purpose, signal intensities of both images were adjusted using Multigauge software to correct for uneven fluorescence yields. The gray scale Cy3 and Cy5 images were separately falsely colored in green or red.

In-solution IEF Fractionation—Between 0.8 and 1.9 mg of protein enriched cell lysates were reconstituted individually in 3.6 ml of an electrofocusing solution prepared with urea, thiourea, DTT, and glycerol OFFGEL kit components for in-solution IEF fractionation of proteins. This solution was prepared as recommended by Agilent except for the use of 1.2% (v/v) pH 3–11 NL IPG buffer (GE Healthcare). 150-μl aliquots of each protein solution were dispensed into the wells of a 24-well OFFGEL sample frame that had been assembled over a 24-cm pH 3–11 NL IPG DryStrip (GE Healthcare) in a tray of the Agilent Technologies 3100 OFFGEL Fractionator according to the accompanying instrument instructions. The samples were focused with a maximum current of 50 μA until 50 kVh were reached using the standard 3100 OFFGEL protein focusing program. Individual wells were subsequently harvested and either used immediately or stored frozen at −20 °C until required.

For analytical purposes, 10-μl aliquots of each fraction were diluted with an equal volume of double concentration reducing sample buffer

and allowed to stand at 22 °C for 2 h prior to one-dimensional SDS-PAGE. Alternatively, after adjustment of the pH of 100 μl of each fraction with 5 μl of 1 M NH_4HCO_3, the proteins were alkylated by the addition of 5 μl of 1 M iodoacetamide and incubation at 22 °C for 2 h in the dark. Reduced and alkylated fractions destined for one-dimensional SDS-PAGE were concentrated by adding 9 volumes of methanol at −20 °C and allowing the proteins to precipitate at −20 °C for 16 h. Precipitated proteins were harvested at 4 °C by centrifugation at 16,000 × *g* for 20 min and reconstituted in a minimal volume of one-dimensional SDS-PAGE sample buffer and separated with 1-mm-thick 12% acrylamide gels using a discontinuous system (42).

Fractions destined for solution digestion were alkylated as above, and 1 μg of trypsin was added immediately prior to the precipitation step. Trypsin co-precipitated samples were washed twice with −20 °C methanol, and residual traces of methanol were evaporated under a gentle stream of dry N_2 gas. Digestion was subsequently initiated by resuspending precipitates in 40 μl of 100 mM NH_4HCO_3 and continued by incubation at 37 °C for 2 h prior to adding another 1 μg of trypsin and continuing the incubation for a further 6 h.

In-gel Digestion—Preparative two-dimensional gels were fixed (30% (v/v) ethanol/10% (v/v) acetic acid) for 45 min, followed by staining overnight using colloidal Coomassie Blue containing 11.8% (v/v) phosphoric acid, 20% (v/v) methanol, 10% (w/v) ammonium sulfate, and 0.12% (w/v) Coomassie Blue G-250 (43). The gels were destained with multiple changes of Milli-Q water to remove the background staining. Scanned gels were either processed immediately or stored in Milli-Q water at 4 °C prior to spot picking. One-dimensional SDS-PAGE gels were either stained with the same colloidal Coomassie method as above or with 0.03% (w/v) Coomassie Blue R-250 in 8% (v/v) acetic acid, 50% (v/v) methanol in water followed by destaining with the same solvent lacking stain and storage in Milli-Q water.

Individual gel plugs were sampled from two-dimensional gels using Eppendorf p-200 pipette tips from which the ends had been severed to create an opening of ~2-mm diameter. The bands were sliced from one-dimensional gels using clean scalpel blades. Gel plugs and bands were washed twice with 100 μl of water and destained twice for 30 min at 37 °C with 100 μl of 40 mM ammonium bicarbonate in 50% (v/v) aqueous ACN and subsequently dehydrated for 10 min in 200 μl of 100% ACN. The dried plugs were rehydrated with 20 μl of trypsin solution (10 ng/μl) in 40 mM NH_4CO_3 (pH 8) and incubated overnight at 37 °C. After overnight incubation, the trypsin solution was collected, and the gel pieces were extracted twice for 30 min with 20 μl of 0.1% (v/v) TFA in 50% (v/v) aqueous ACN. The trypsin supernatant and extracts were pooled and reduced to approximately one-third of the original volume in a vacuum centrifuge.

MALDI-TOF/TOF-MS/MS Analysis—All of the mass spectra were acquired in positive ion mode on an Ultraflex III MALDI-TOF/TOF instrument (Bruker Daltonics) as described previously (44, 45). In-gel digests were further concentrated by adsorption to and elution from C18 ZipTips® (Millipore, Bedford) according to a published protocol (46). Aliquots of ZipTip® eluates (1 μl) were mixed with α-cyano-4-hydroxy cinnamic acid matrix (2 μl), and 1.5-μl aliquots of the mixtures were applied to a MTP format stainless steel target plate. The spectra were calibrated using a peptide calibration standard mixture (Bruker Daltonics) of nine peptides in the mass range of m/z = 1046 and m/z = 3147 (44, 45). Protein identification was performed by database searching of a custom human and virus database using an in-house Mascot server (Matrix Science). Searches were submitted to Mascot (version 2.2.06) using BioTools™ (Bruker Daltonics; version 3.2). The custom database consisted of the complete proteome sets for *Homo sapiens*, *Bos taurus*, and strain A2 of hRSV and proteins matching GFP. The database of 80,707 protein sequences was downloaded from Uniprot (www.uniprot.org) on July 27, 2011. The Mascot search parameters were: enzymatic cleavage set to tryptic (allowing a maximum of two missed cleavages) and carbamidomethylation of cysteine specified as a fixed modification. Deamidation of asparagine/glutamine and methionine oxidation were specified as variable modifications. Fragment ion and parent ion mass tolerances were set to 0.8 Da and 75 ppm, respectively.

Most protein identifications were based on two matching peptide MS/MS spectra with Expected values (E-values) of less than 0.05 (supplemental Table 2) and additional peptide spectra with E-values of less than 0.05 and/or an additional peptide(s) with a less confident E-value(s). Where identifications were based on only one peptide spectrum with an E-value of less than 0.05 or multiple MS/MS spectra with less confident E-values, MS/MS spectra are presented in supplemental Fig. 3. The principle of parsimony was applied for protein identification.

Capillary HPLC-LTQ-Orbitrap—In-gel or solution tryptic digests were subjected to CapHPLC-MS/MS analysis using an UltiMate 3000 HPLC system (Dionex) interfaced with a linear ion trap (LTQ)-Orbitrap XL hybrid mass spectrometer (Thermo Fisher Scientific, Bremen, Germany). Aliquots (7 μl) of tryptic digests were acidified with 1 μl of 50% (v/v) aqueous formic acid and loaded onto a 300 Å, 300-μm × 5-mm C18 trap column (Dionex Acclaim® PepMap™ μ-Precolumn) at 20 μl/min in 98% solvent A (0.1% (v/v) aqueous formic acid) and 2% solvent B (80% (v/v) ACN/20% (v/v) H_2O containing 0.1% (v/v) formic acid) for 5 min at 40 °C and subsequently back flushed onto a pre-equilibrated analytical column (Vydac Everest C18 300Å, 150 μm × 150 mm; Alltech) using a flow rate of 1 μl/min. After washing the analytical column at 0% B for 5 min, the peptides were separated at 40 °C using a sequence of linear gradients: to 45% B over 75 min; to 75% B over 15 min; and, to 100% B over 5 min and then holding the column at 100% B for 10 min. Eluates from the analytical column were introduced into the LTQ-Orbitrap throughout the entire run via a dynamic nano-electrospray ion source (Proxeon, Odense, Denmark) containing a 30-μm-inner diameter uncoated silica emitter (New Objective). Typical spray voltages were between 1.4 and 1.8 kV, and no sheath, sweep, or auxiliary gases were used. The heated capillary temperature was set to 200 °C. The LTQ-Orbitrap XL was controlled using Xcalibur 2.0 software (Thermo Fisher Scientific) and operated in a data-dependent acquisition mode to automatically switch between Orbitrap-MS and ion trap-MS/MS. The survey full scan mass spectra (m/z 300–2000) were acquired in the Orbitrap with a resolving power set to 60,000 (at 400 m/z) after accumulating ions to an automatic gain control target value of 5.0 × 10^5 charges in the LTQ. MS/MS spectra were concurrently acquired on the eight most intense ions from the survey scan in the LTQ filled to an automatic gain control target value of 3.0 × 10^4. Charge state filtering, where unassigned precursor ions were not selected for fragmentation, and dynamic exclusion (repeat count, 1; repeat duration, 30 s; exclusion list size, 500; and exclusion duration, 35 s) were used. Fragmentation conditions in the LTQ were: 35% normalized collision energy, activation q of 0.25, 30-ms activation time, and minimum ion selection intensity 1000 counts. Maximum ion injection times were 500 ms for survey full scans and 100 ms for MS/MS.

Tandem mass spectra were searched using the same general search parameters and the database described above in the "MALDI-TOF/TOF-MS/MS analysis" section. The searches were submitted to Mascot using Proteome Discoverer (Thermo Fisher Scientific; version 1.3). Fragment and parent ion mass tolerances were set to 0.8 Da and 20 ppm, respectively. E-values of less than 0.05 were used as criteria for confident peptide identifications.

Western Blot Analysis—Proteins were separated by one-dimensional SDS-PAGE, transferred to PVDF (0.2 μm) membrane (Millipore or Bio-Rad) and blocked with 1% (w/v) BSA in buffer comprising 10 mM Tris-HCl (pH 7.4) and 0.15 M NaCl (TBS) with 0.5% (v/v) Tween 20 (TBST). The membranes were washed with TBS and TBST and

probed by incubation with primary antibodies specific for SOD2 (1:4000), IFIT3 (1:1000), CAT (1:1000), STAT1 (1:4000), STAT2 (1:500), NRF2 (1:1000), TXNRD1 (1:2000), or a polyvalent antibody to hRSV (1:1000) diluted in 4% (w/v) skim milk powder in TBS or 1% (w/v) BSA in TBST. The membranes were washed thoroughly with TBS and TBST, and bound antibodies were detected using anti-rabbit IgG-conjugated IR680, anti-mouse or anti-goat IgG conjugated with IR800 (1:5000 to 1:20,000) in 4% (w/v) skim milk powder in TBS or 1% BSA in TBST. Membranes were washed thoroughly with TBS, scanned using an Odyssey Infrared Imaging System (LI-COR), and analyzed quantitatively. Multiple independent biological replicates were analyzed for each experiment using Graphpad Prism as indicated in the figure legends. Protein samples were enriched and quantified as described above, and equivalent protein quantities were loaded onto gels for each sample in all experiments. Equivalent loading and transfer were validated using SyproRuby® as a quantitative membrane protein stain followed by densitometry and destaining prior to the blocking step of the blotting protocol (47). Densitometry for each SyproRuby-stained lane was measured to determine statistically equivalent loading for each experiment. Total protein staining was preferred over selection of a host cell protein as a loading control because protein expression may have been regulated by WT-GFP hRSV and ΔNS1-GFP hRSV infection. The same statistical treatment was applied to validate the protein staining as was used above for the blotting data.

Quantitative RT-PCR—For quantitative real time PCR analysis of SOD2 mRNA, A549 cells in 6-well plates were infected with the viruses at multiplicity of infection of 3 plaque-forming units/cell. At 24 h postinfection, total RNA was isolated by RNEasy RNA isolation kit (Qiagen), and cDNA was synthesized using Super Script III reverse transcriptase (Invitrogen) according to the manufacturer's recommendations. SOD2 cDNA was analyzed by quantitative real time PCR using Platinum PFX (Invitrogen) and a TaqMan primer and probe set designed from the known SOD2 sequence (GenBank™ accession number Hs00167309_m1) (Invitrogen) according to the manufacturer's recommendations. Human β-actin was used as the endogenous control for each sample (Invitrogen catalogue number 4333762F). The $2^{-\Delta\Delta C_T}$ method (48) was used to calculate the relative increase of SOD2 mRNA in virus-infected compared with mock infected cells. ΔC_t values were calculated for each sample, and the mean C_t values were calculated for each treatment.

RESULTS

Deletion of NS1 from the hRSV Genome Enhances Expression of Specific Cellular Proteins in Response to Infection and Attenuates hRSV Replication—Immortalized human A549 type II alveolar epithelial cells (49, 50) are widely used to study the infectious properties of human respiratory viruses (31, 32). Consequently, these cells were used in conjunction with two-dimensional DIGE to analyze the impact of NS1 on the host cell response to hRSV infection at a proteomic level.

A549 cells were infected at a multiplicity of infection of 3 plaque-forming units/cell in three or more independent biological replicate experiments with WT-GFP hRSV or ΔNS1-GFP hRSV or were mock infected, and the cells were incubated for 24 h and processed for two-dimensional DIGE (supplemental Table 1). Fusion of all gels from this experimental protocol resulted in detection of 1681 discrete spots. Compared with mock infected cells, WT-GFP hRSV-infected cells had 58 protein spots statistically significantly differentially regulated at $\alpha < 0.01$ and a fold difference of 1.2 or greater (supplemental Fig 1*A*). Comparison of ΔNS1-GFP hRSV-infected and mock infected cells (supplemental Fig. 1*B*) revealed 124 statistically significantly regulated spots and differences between the spots regulated by WT-GFP hRSV-infected compared with mock infected cells. Comparison of ΔNS1-GFP hRSV- and WT-GFP hRSV-infected cells essentially resulted in an amalgam of the comparisons of these two infectious circumstances to mock infection (Fig. 1).

Protein spots observed to be statistically significantly regulated were excised from Coomassie-stained preparative gels of unlabeled lysates of WT-GFP hRSV-infected (supplemental Fig. 2*A*) and ΔNS1-GFP hRSV-infected cells (supplemental Fig. 2*B*) and attempts made to identify these proteins after in-gel digestion by MALDI-TOF/TOF-MS/MS. Thirty-six of the statistically significantly regulated spots (Table I and supplemental Table 2) yielded identifications of interest after excluding differential carryover of bovine proteins from media during sample preparation (data not shown). The spots from which identifications were made are indicated on the two-dimensional DIGE comparison of ΔNS1-GFP hRSV- and WT-GFP hRSV-infected cells (Fig. 1). Eleven of these spots contained proteins that were products of the genomes of the hRSV clones used for infections, including GFP isoforms. The remaining statistically significantly regulated spots contained 22 nonredundant human cellular proteins that were of interest because of their apparent regulation by NS1 (*i.e.* generally suppression), indicating that NS1 interacted with them directly or affected members of pathways required for their expression.

Only spot 2 revealed more than one protein identification (LGALS3 and hRSV M) based on the criteria specified under "Experimental Procedures." It should be noted that five of the regulated proteins listed in Table I were included on the basis of only one MS/MS spectrum with an E-value of less than 0.05 (supplemental Table 2). Only one identification (APOL2 in spot 22) was based on MS/MS spectra for peptides (3) with E-values of greater than 0.05 (Fig. 1, Table I, and supplemental Table 2); these spectra are presented in supplemental Fig. 3. APOL2 was subsequently identified from the corresponding spot from lysates of IFN-γ-treated cells (see below; supplemental Fig. 8*B*) based on finding a peptide common to the spot 22 of the infected cell lysate but that revealed an E-value of less than 0.05 and another peptide from APOL2 with an E-value of 0.086 (supplemental Fig. 3*G*). The extents of regulation of the identified proteins are presented (Fig. 2, Table I, and supplemental Tables 3–5).

In the comparison of the WT-GFP hRSV-infected cells with mock infected cells, only 13 regulated protein spots could be identified with confidence. Proteins in eight of these spots were viral in origin and featured as being up-regulated (Fig 2*A*, Table I, and supplemental Table 3). Only two cellular proteins were found to be regulated by WT-GFP hRSV infection. These proteins, cytoplasmic thioredoxin reductase 1 and actin-related protein 3 were down-regulated. A third cellular protein, galec-

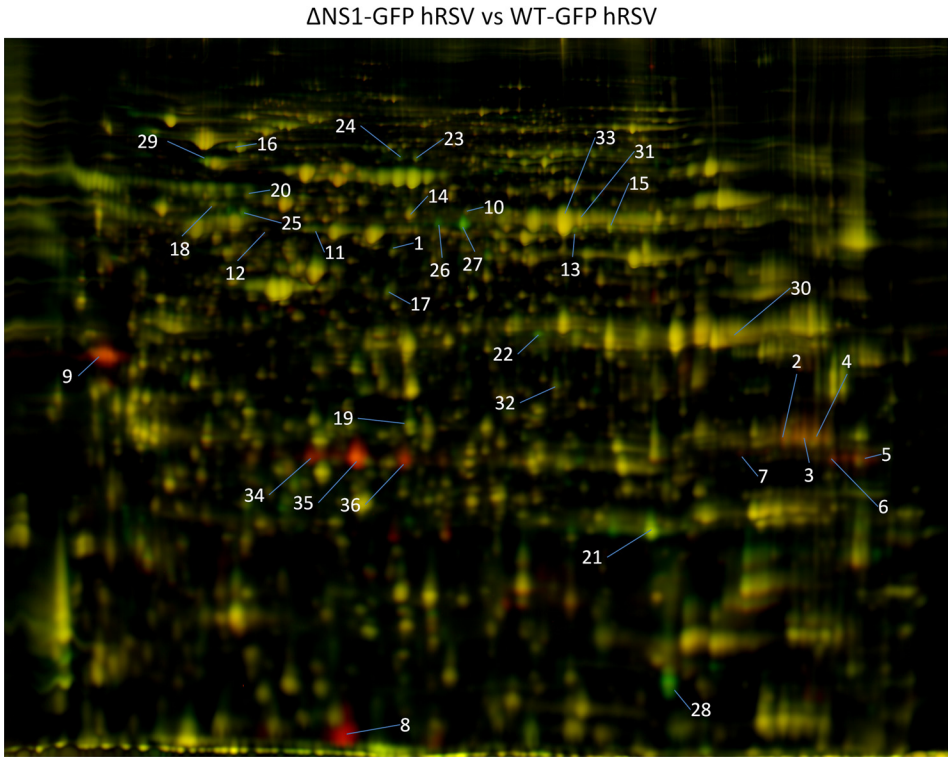

FIG. 1. **Comparisons of proteomes of A549 cells infected with ΔNS1-GFP hRSV and WT-GFP hRSV by two-dimensional DIGE.** The image depicted is for gel 1 described in supplemental Table 1. The *numbered red spots* indicate proteins whose abundance appeared to increase in response to WT-GFP hRSV compared with ΔNS1-GFP hRSV, and the converse is true for *numbered green spots*.

tin-3, was identified from regulated spot 3 (Fig. 1), but as mentioned above this spot contained the viral matrix protein that was evident in other spots because of infection, and post-translational modifications probably accounted for the regulation of this spot. Three of the up-regulated proteins were identified as GFP, which arose from replication of the viral genome, which included GFP as an inserted gene (Fig. 1 and Table I).

As expected from a visual inspection of the data presented in Fig. 1, a much higher degree of statistically significant protein regulation was apparent in a comparison of ΔNS1-GFP hRSV- and WT-GFP hRSV-infected cells (Fig. 2*B*, Table I, and supplemental Table 4). This quantitative comparison indicated two distinct trends of regulation. Proteins derived by expression of viral genes, such as M (human respiratory syncytial virus matrix protein), P (human respiratory syncytial virus phosphoprotein), and NS1 and GFP, evident in 11 spots, predominated in the WT-GFP hRSV-infected cell lysates. On the other hand, cellular proteins were relatively more abundant in 21 spots from the ΔNS1-GFP hRSV-infected cells compared with WT-GFP hRSV-infected cells (Fig. 2*B*, Table I, and supplemental Table 4). This indicated that although ΔNS1-GFP hRSV replicates much more poorly than WT-GFP hRSV, it elicits a much more profound cellular response to infection.

Consistent with the observations above, when the data from the ΔNS1-GFP hRSV-infected and mock infected lysates were directly compared, the viral phosphoprotein was the only hRSV protein evident in this comparison, and only one GFP-containing spot was evident (Fig. 2*C*, Table I, and supplemental Table 5). In contrast, 21 regulated spots evident in this comparison contained cellular proteins (Fig. 2*C*, Table I, and supplemental Table 5). Three of these cellular protein spots were down-regulated, and the remaining 18 were up-regulated as a consequence of deleting NS1 from the hRSV genome (Fig. 2*C*, Table I, and supplemental Table 5).

Of the 22 cellular proteins that were differentially regulated by the removal of NS1, data exist (50) or were obtained later in this study by direct cytokine stimulation to indicate whether their expression is inducible by type I, type II, and/or type III IFNs or likely to be affected by other regulators (Table II).

Only one NS1-regulated protein, SERPINB9, appears to be uniquely regulated by a type I IFN (*i.e.* IFN-β; Table II), and one protein, G6PD, appears to be uniquely regulated by a type III IFN (*i.e.* IFN-λ1; Table II). The ubiquitin-like protein, ISG15, did not exhibit regulation in WT-GFP hRSV-infected compared with mock infected A549 cells (Table I) but was substantially up-regulated upon deletion of NS1 (Fig. 1, *spot 28*; and Table I). This protein is regulated by either type I (IFN-β) or type III (IFN-λ1) IFNs (Table II). Regulation of the three abovementioned proteins by NS1 implies an impact on signaling mediated by the heterodimeric STAT1/STAT2 transcription factor.

TABLE I

Regulation data for proteins detected as being regulated in A549 cells as a consequence of infection with WT-GFP hRSV or ΔNS1-GFP hRSV, for which identities were determined

UniprotKB	UniprotKB protein name	Spot number on two-dimensional DIGE image	Regulation[a]		
			WT-GFP hRSV/mock	ΔNS1-GFP hRSV/mock	ΔNS1-GFP hRSV/ WT-GFP hRSV
P61158	Actin-related protein 3	1	−1.32	NSS	1.53
P03419	Matrix protein (hRSV)	2	4.42	NSS	−3.69
		3	8.14	NSS	−5.09
		4	8.01	NSS	−3.31
P04545	Matrix M2–1 (hRSV)	5	5.19	NSS	−5.26
		6	4.49	NSS	−5.47
		7	2.87	NSS	−2.92
P04544	NS1 (hRSV)	8	6.42	NSS	−7.47
P03421	Phosphoprotein (hRSV)	9	88.4	5.39	−16.4
Q16881	Thioredoxin reductase 1, cytoplasmic	10	−1.22	NSS	1.56
P08729	Keratin, type II cytoskeletal 7	11	NSS	1.47	−3.04
		12	NSS	NSS	1.53
P28838	Cytosol aminopeptidase	13	NSS	NSS	1.21
P30101	Protein disulfide-isomerase A3	14	NSS	1.27	1.24
P43490	Nicotinamide phosphoribosyltransferase	15	NSS	1.20	1.25
P21980	Protein-glutamine γ-glutamyltransferase 2	16	NSS	1.73	1.52
P50453	Serpin B9	17	NSS	1.78	1.53
P31150	Rab GDP dissociation inhibitor α	18	NSS	1.49	1.58
Q06323	Proteasome activator complex subunit 1	19	NSS	1.74	1.67
P61978	Heterogeneous nuclear ribonucleoprotein K	20	NSS	1.75	1.68
P04179	Superoxide dismutase (Mn), mitochondrial	21	NSS	3.55	2.37
Q9BQE5	Apolipoprotein L2	22	NSS	2.60	2.45
P20591	Interferon-induced GTP-binding protein Mx1	23	NSS	4.31	2.48
		24	NSS	5.28	3.17
O14879	Interferon-induced protein with tetratricopeptide repeats 3	25	NSS	2.83	4.23
P23381	Tryptophanyl-tRNA synthetase, cytoplasmic	26	NSS	2.31	2.81
		27	NSS	5.64	5.91
P05161	Ubiquitin-like protein ISG15	28	NSS	4.30	3.62
P11021	78-kDa glucose-regulated protein	29	NSS	2.44	2.50
P42330	Aldo-keto reductase family 1 member C3	30	NSS	−1.31	−1.17
P11413	Glucose-6-phosphate 1-dehydrogenase	31	NSS	−1.19	−1.09
P00491	Purine nucleoside phosphorylase	32	NSS	1.29	1.24
P00352	Retinal dehydrogenase 1	33	NSS	−1.21	NSS
P42212	Green fluorescent protein	34	9.13	1.02	−8.93
		35	32.7	1.58	−20.7
		36	4.64	−1.43	−6.65

[a] NSS indicates lack of statistically significant difference when data from all relevant gels taken into account.

Eight of the NS1-regulated proteins are regulated by different combinations of type I (IFN-α and/or -β), type II (IFN-γ), and/or type III (IFN-λ1) IFNs (Table II). These findings support the notion that NS1 impacts on STAT1/STAT2-mediated signaling and implies that NS1 also regulates signaling mediated by the homodimeric STAT1/STAT1 transcription factor. One of this class of proteins (LAP3, isoform 1 of cytosol aminopeptidase) that is induced by type I and type II IFNs was not statistically significantly different between WT-GFP hRSV- or ΔNS1-GFP hRSV-infected and mock infected cells but was significantly higher in abundance in ΔNS1-GFP hRSV-infected cells compared with WT-GFP hRSV-infected cells (Fig. 2*B*, Table I, and supplemental Table 4).

Four of the NS1-regulated proteins were uniquely type II (IFN-γ)-inducible proteins; thus, strengthening the probability that NS1 has the ability to directly impact on STAT1/STAT1 mediated signaling (Table II). Interestingly, six of the NS1-regulated proteins have not been observed to be regulated by IFNs; thus, raising the possibility that NS1 regulates their expression via direct impacts on these proteins and/or impacts on signaling pathways, other than IFN signaling, involved in their expression. Overall these findings are consistent with previous conclusions that NS1 suppresses type I and III IFN and other antiviral responses (28, 31, 32, 36, 37, 51) and may explain the attenuation of ΔNS1-GFP hRSV. Furthermore, it is apparent from the present study that NS1 suppresses type II IFN signaling.

Of the uniquely IFN-γ-inducible proteins that were regulated by NS1, SOD2 exhibited the largest degree of suppression by NS1. This finding focused attention on SOD2 for downstream aspects of the present study because of potential implications for regulation of oxidative stress during hRSV infection and the potential for NS1 to regulate STAT1/STAT1 signaling.

Proteomic Confirmation That SOD2 Is Regulated by NS1—One critical observation made above was that SOD2 ap-

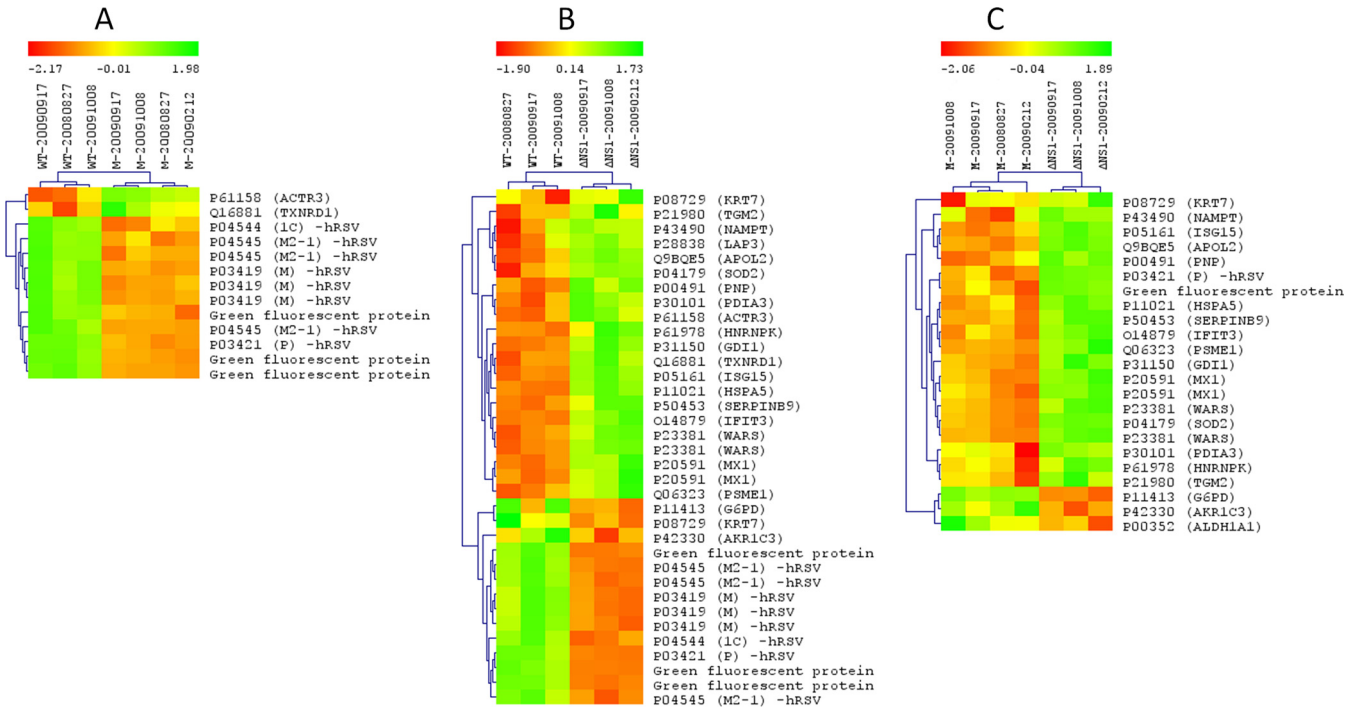

FIG. 2. **Heat map comparisons of differential protein expression in lysates of mock infected and WT-GFP hRSV- and ΔNS1-GFP hRSV-infected A549 cells determined by quantitative two-dimensional DIGE.** The heat maps represent comparisons of mock with WT-GFP hRSV (*A*), WT-GFP hRSV with ΔNS1-GFP hRSV (*B*), and mock with ΔNS1-GFP hRSV (*C*) infections, respectively. Relative spot intensities can be determined from the scales presented above each respective heat map. The accession numbers and gene names are presented to the *right* of each heat map.

TABLE II
Impact of IFNs on NS1-regulated proteins in A549 cells

Uniprot protein name	Gene name	IFN regulators
Serpin B9	SERPINB9	β
Glucose-6-phosphate 1-dehydrogenase	G6PD	λ
Ubiquitin-like protein ISG15	ISG15	$\beta\lambda$
Aldo-keto reductase family 1 member C3	AKR1C3	$\beta\gamma$
Protein-glutamine γ-glutamyltransferase 2	TGM2	$\beta\gamma$
Interferon-induced GTP-binding protein Mx1	MX1	$\alpha\beta\gamma\lambda$
Interferon-induced protein with tetratricopeptide repeats 3	IFIT3	$\alpha\beta\gamma\lambda$
Cytosol aminopeptidase	LAP3	$\alpha\beta\gamma$
Apolipoprotein L2	APOL2	$\beta\gamma$
Proteasome activator complex subunit 1	PSME1	$\beta\gamma\lambda$
Tryptophanyl-tRNA synthetase, cytoplasmic	WARS	$\beta\gamma\lambda$
Keratin, type II cytoskeletal 7	KRT7	$\gamma\lambda$
Superoxide dismutase [Mn], mitochondrial	SOD2	γ
Thioredoxin reductase 1, cytoplasmic	TXNRD1	γ
Protein disulfide-isomerase A3	PDIA3	γ
78-kDa glucose-regulated protein	HSPA5	γ
Actin-related protein 3	ACTR3	–
Nicotinamide phosphoribosyltransferase	NAMPT	–
Rab GDP dissociation inhibitor α	GDI1	–
Heterogeneous nuclear ribonucleoprotein K	HNRNPK	–
Purine nucleoside phosphorylase	PNP	–
Retinal dehydrogenase 1	ALDH1A1	–

peared to be regulated by NS1. As mentioned above, exposure of A549 cells to type II IFN but not type I IFN was shown to induce SOD2 (50); however, another study indicated that massive doses of IFN-α induced SOD2 in rodent hepatic stellate cells (52). Despite the fact that the spot that contained SOD2 was quite intensely stained by Coomassie Blue and

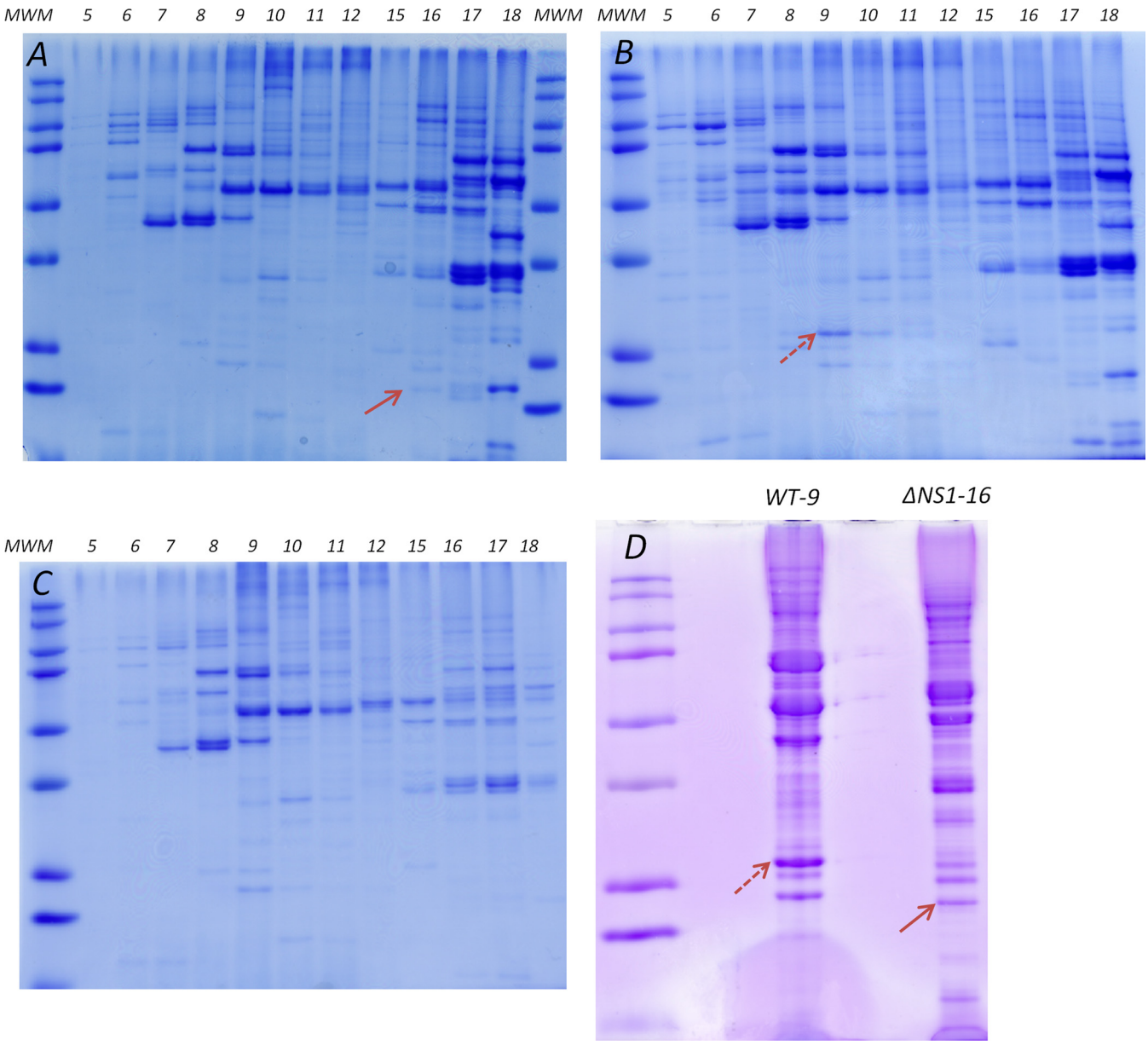

FIG. 3. **Fractionation of infected A549 cell lysates by in-solution IEF.** *A–C*, lysates of ΔNS1-GFP hRSV-infected (1.22 mg) (*A*), WT-GFP hRSV-infected (1.86 mg) (*B*), or mock infected (0.83 mg) (*C*) A549 cells were individually subjected to IEF fractionation in solution in a pH 3–11 nonlinear gradient. Individual fractions were harvested, and aliquots were subjected to analytical one-dimensional SDS-PAGE followed by staining with colloidal Coomassie. Proteins in fractions of interest were precipitated with cold methanol to obtain samples of increased protein concentrations for one-dimensional SDS-PAGE. *D*, results of separation of concentrated proteins from fractions 16 and 9 of the IEF separations of the ΔNS1-GFP hRSV-infected (ΔNS1–16) and WT-GFP hRSV-infected (WT-9) cell lysates, respectively, visualized using standard Coomassie staining. *MWM* indicates molecular weight marker lanes. *Solid arrows* on lanes labeled *ΔNS1–16* and *dashed arrows* on lanes labeled *WT-9* indicate bands correspond to SOD2 and GFP, respectively.

exhibited strong induction by infection of A549 cells with ΔNS1-GFP hRSV (Fig. 1, Table I, and supplemental Fig. 2*B*), the identification of SOD2 was based on only one distinct peptide (supplemental Table 2 and supplemental Fig. 3*C*). Thus, additional larger scale fractionation was performed on the digests to obtain a more confident identification of SOD2 and to confirm its regulation by NS1 rather than that of a potentially co-migrating protein. This involved in-solution IEF separation of individual lysates of ΔNS1-GFP hRSV- and WT-GFP hRSV-infected and mock infected A549 cells followed by one-dimensional SDS-PAGE. Analytical scale one-dimensional SDS-PAGE of aliquots of the IEF fractions revealed an apparent increase in the abundance of a Coomassie-stained band corresponding to SOD2 in fraction 16 of the ΔNS1-GFP hRSV-infected cell lysate (Fig. 3*A*, *solid red arrow*) compared with fractions 16 from WT-GFP hRSV-infected (Fig. 3*B*) and

mock infected (Fig. 3*C*) lysates. Specifically, the one-dimensional SDS-PAGE protein profile of this fraction (Fig. 3*A*) was very similar to that expected for a vertical slice through the pI region of the Coomassie-stained two-dimensional gels (supplemental Fig. 2) that contained SOD2. The bulk of fraction 16 was concentrated by methanol precipitation followed by one-dimensional SDS-PAGE, and the band of interest (Fig. 3*D*, *lane ΔNS1–16*) was subjected to in-gel digestion. MALDI-TOF/TOF-MS/MS analysis followed by database searching led to confident identification of this protein as SOD2 (supplemental Table 6). To support this identification, aliquots of fraction 16 from the preparative in-solution IEF separations of mock infected and WT-GFP hRSV- and ΔNS1-GFP hRSV-infected cell lysates were individually subjected to solution digestion followed by CapHPLC-LTQ-Orbitrap-MS/MS. SOD2 was confidently identified in fraction 16 of the ΔNS1-GFP hRSV-infected cell lysate. Five distinct tryptic peptides derived from SOD2 were identified in this fraction (supplemental Table 7). By comparison, only one of these unique SOD2 tryptic peptides was identified in fractions 16 from mock infected and WT-GFP hRSV-infected cell lysates (supplemental Table 7). Furthermore, the number of spectra that matched SOD2 (*i.e.* the spectral count) suggested that SOD2 was dramatically more abundant in the lysate of the ΔNS1-GFP hRSV-infected cells compared with mock infected and WT-GFP hRSV-infected cells (supplemental Table 7).

The analytical scale one-dimensional SDS-PAGE analysis of the fractions from the large scale in-solution IEF separations also identified a band of interest in fraction 9 from WT-GFP hRSV-infected cell lysates (Fig. 3*B*, *dashed arrow*). A portion of this fraction was concentrated and subjected to one-dimensional SDS-PAGE, and the band was identified as GFP by in-gel digestion followed by MALDI-TOF/TOF-MS/MS (Fig. 3*D*, *lane WT-9*, and supplemental Table 6). The presence of GFP in fraction 9 of the WT-GFP hRSV-infected cell lysate was consistent with the pI position of the major red spot (spot 35) on two-dimensional DIGE gels of this lysate (Fig. 1) as was the correspondence between the apparent M_r of this red spot (Fig. 1) and the M_r of GFP (Fig. 3, *B* and *D*). GFP appeared to be more abundant in WT-GFP hRSV-infected cell lysate than in the lysates of mock infected and ΔNS1-GFP hRSV-infected cells, as indicated by the *dashed arrow* on the SDS-PAGE analysis of fraction 9 of the WT-GFP hRSV-infected cell lysate (Fig. 3*B*). The greater abundance of GFP in fraction 9 of the WT-GFP hRSV-infected cell lysate than in the mock infected and ΔNS1-GFP hRSV-infected cell lysates was supported by the greater number of spectra corresponding to GFP found by CapHPLC-LTQ-Orbitrap analysis of solution digests of the individual fractions 9 (supplemental Table 7). These data support the conclusion above that SOD2 is the protein in spot 21 whose expression is regulated by NS1. Furthermore, the data indicate that WT-GFP hRSV replicates more efficiently than ΔNS1-GFP hRSV.

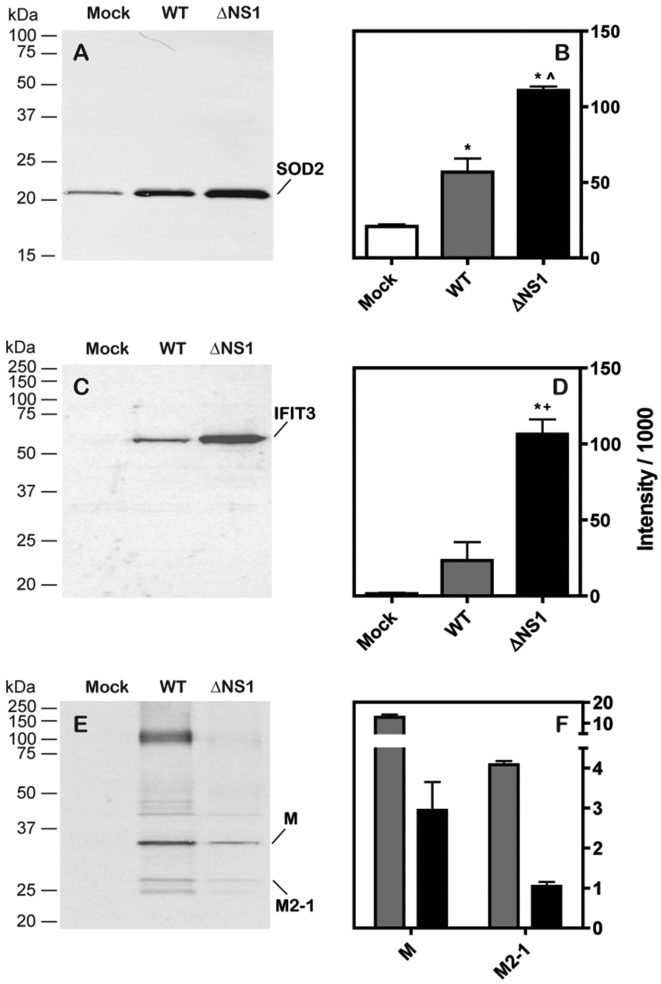

FIG. 4. **Western blot analysis of SOD2, IFIT3, and hRSV M and M2-1 proteins in lysates of mock infected or WT-GFP hRSV- or ΔNS1-GFP hRSV-infected A549 cells.** Equal quantities of protein from lysates of WT-GFP hRSV- or ΔNS1-GFP hRSV-infected or mock infected A549 cells were analyzed by Western blotting for SOD2 (*A* and *B*), IFIT3 (*C* and *D*), and hRSV proteins (*E* and *F*). Four independent sets of infected samples were measured in triplicate, with representative Western blots shown in *A*, *C*, and *E*. Normalized integrated intensities for SOD2 (*B*) and IFIT3 (*D*) in mock infected (*Mock*), WT-GFP hRSV-infected (*WT*), and ΔNS1-GFP hRSV-infected (*ΔNS1*) samples are presented as the means ± S.E. ($n = 4$). Statistical analysis was performed using one-way ANOVA for SOD2 and IFIT3 with Bonferroni correction. * and ^ denote a statistically significant difference from mock and WT infection, respectively, at $p < 0.05$. + denotes a statistical difference from WT infection at $p < 0.10$. In *F*, the integrated fluorescent intensities of the hRSV M and M2-1 proteins from the WT-GFP hRSV (*gray*) and ΔNS1-GFP hRSV lysates (*black*) are presented. Verification of equivalent protein loading was achieved using SyproRuby staining as shown in supplemental Fig. 4.

Orthogonal Validation That SOD2 Is Regulated by NS1—Lysates of mock infected and WT-GFP hRSV- and ΔNS1-GFP hRSV-infected A549 cells were analyzed by Western blotting using a SOD2-specific antibody (Fig. 4*A*). As opposed to quantitative two-dimensional DIGE analysis, quantitative Western blotting indicated that SOD2 immunoreactivity was

statistically significantly increased in lysates of WT-GFP hRSV-infected cells compared with lysates of mock infected cells (Fig. 4*B*). However, as with two-dimensional DIGE, SOD2 levels were found to be further increased in ΔNS1-GFP hRSV-infected cell lysates by quantitative Western blotting (Fig. 4*B*). Comparison of levels of the IFN-induced protein, IFIT3, identified in spot 25 (Fig. 1, Table I, and supplemental Table 2), in infected cells relative to mock infected cells by quantitative Western blotting (Fig. 4, *C* and *D*) indicated the same qualitative trend in expression as observed qualitatively and quantitatively for SOD2 in WT-GFP hRSV- and ΔNS1-GFP hRSV-infected cell lysates (Fig. 4, *A* and *C*). Quantitative analysis showed that IFIT3 levels were increased in WT-GFP hRSV-infected compared with mock infected cells and were higher again in ΔNS1-GFP hRSV-infected compared with WT-GFP hRSV-infected cell lysates (Fig. 4*D*).

Western blot analysis of the infected cell lysates using a polyclonal antiserum prepared against hRSV virions confirmed the results of the two-dimensional DIGE analyses (Fig. 1) that showed higher levels of expression of virally encoded proteins for WT-GFP hRSV compared with ΔNS1-GFP hRSV, as represented by the expression of hRSV M and M2-1 proteins detected by Western blotting (Fig. 4, *E* and *F*). Thus, the higher levels of SOD2 and IFIT3 expressed in response to ΔNS1-GFP hRSV compared with WT-GFP hRSV were not a direct reflection of the general level of viral protein expression, because the expression of viral protein by ΔNS1-GFP hRSV in A549 cells was ~0.25-fold that of WT-GFP hRSV at 24 h, but the levels of SOD2 in cell lysates were 2.6 times higher. These data indicate that the higher levels of SOD2 expression in the attenuated ΔNS1-GFP hRSV are attributable to the lack of NS1. This was supported by findings with FlagNS1 hRSV (supplemental Fig. 5), which exhibits similar replicative characteristics to WT hRSV (a recombinant clone of human respiratory syncytial virus containing the wild-type A2 subtype genome). SOD2 expression in FlagNS1 hRSV-infected A549 cells was proportional to the level of M and M2-1 protein expression over a 6–30-h period (supplemental Fig. 5*B*), and the fold changes in SOD2 at 24 h were comparable for WT-GFP hRSV (Fig. 4*B*) and FlagNS1 hRSV (supplemental Fig. 5*B*).

The induction of SOD2 observed in WT-GFP hRSV-infected A549 cells by Western blotting is consistent with other reports on SOD2 in WT hRSV-infected cells (40). Failure to detect this induction in WT-GFP hRSV-infected A549 cells by DIGE apparently reflects a deficiency in the sensitivity of DIGE under the current experimental conditions or that SOD2 might have been distributed across more spots than spot 21 because of post-translational modifications.

SOD2 mRNA levels, determined in two separate complementary quantitative real time PCR analyses of mRNA extracted from the lysates of A549 cells that were mock infected or WT-GFP hRSV- or ΔNS1-GFP hRSV-infected for 24 h (supplemental Fig. 6), mirrored the trend in relative SOD2

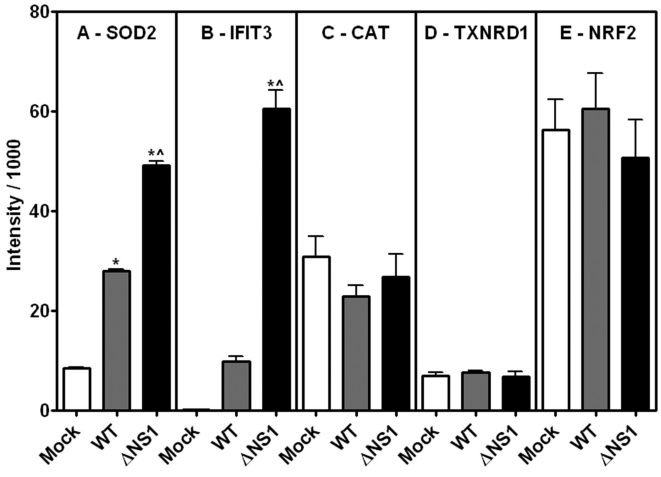

FIG. 5. **Expression of SOD2 (*A*), IFIT3 (*B*), catalase (*C*), TXNRD1 (*D*), and NRF2 (*E*) in mock infected and WT-GFP hRSV- and ΔNS1-GFP hRSV-infected A549 cells.** Equal quantities of protein from lysates of WT-GFP hRSV- or ΔNS1-GFP hRSV-infected or mock infected A549 cells were analyzed by Western blotting for SOD2 (*A*), IFIT3 (*B*), CAT (*C*), TXNRD1 (*D*), and NRF2 (*E*). The data were normalized using SOD2 or IFIT3 levels present in a lysate of either FlagNS1 hRSV-infected (SOD2, IFIT3, and CAT) or IFN-β-treated (TXNRD1 and NRF2) A549 cells loaded in triplicate on the same membrane as the treatment. Normalized integrated intensities are shown as the means ± S.E. for four independent sets of treated samples measured in triplicate ($n = 4$). Statistical analysis was performed using a one-way ANOVA with Bonferroni correction. * and ^ denote a statistically significant difference from mock and WT infection, respectively, at $p < 0.05$. Mock infected and WT-GFP hRSV- and ΔNS1-GFP hRSV-infected cells are represented by *open*, *gray*, and *black bars*, respectively.

protein levels determined by quantitative two-dimensional DIGE and Western blotting. These data confirmed that SOD2 is the protein in spot 21 whose expression is regulated by NS1 and that WT-GFP hRSV replicates more efficiently than ΔNS1-GFP hRSV and are consistent with NS1 being a regulator of SOD2 expression in hRSV-infected A549 cells.

NS1 Does Not Regulate the NRF2 Oxidative Stress Response Pathway—Infection of A549 cells by RSV has previously been reported to modulate expression of oxidative stress response enzymes, including SOD2, that are under the control of the NRF2 transcription factor (40, 53). The potential for the suppression of SOD2 expression by NS1 observed in the present study being a result of an impact on the NRF2 pathway was investigated by measuring the levels of two enzymes in addition to SOD2, catalase and TXNRD1, which are also regulated by NRF2. NRF2 levels were also measured. Quantitative Western blotting using three new sets of independent biological replicates of mock infected and WT-GFP hRSV- and ΔNS1-GFP hRSV-infected A549 cells indicated that SOD2 (Fig. 5*A*) and IFIT3 (Fig. 5*B*) levels in these samples exhibited the same trend in regulation that was observed above for the earlier sets of replicates, but catalase (Fig. 5*C*) and TXNRD1 (Fig. 5*D*) were the same in all circumstances. Furthermore, NRF2 did not exhibit any differential expression

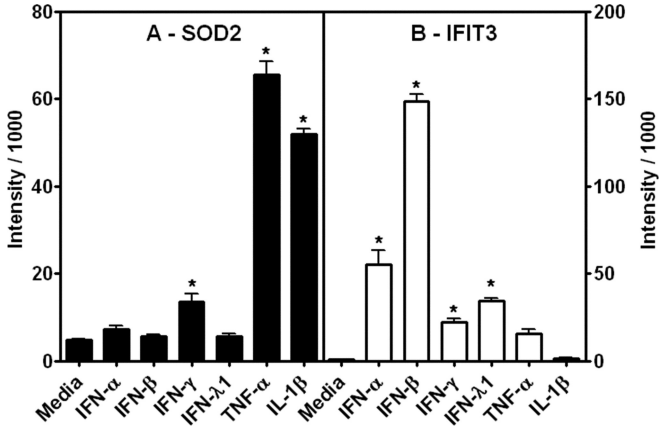

FIG. 6. **Up-regulation of SOD2 (*A*) and IFIT3 (*B*) protein expression in A549 cells by IFN-α, IFN-β, IFN-γ, IFN-λ1, TNF-α, and IL-1β.** A549 cells were incubated for 24 h in the presence of 500 units/ml of IFN-α and IFN-β, 100 ng/ml of IFN-γ, 100 ng/ml of IFN-λ1, 20 ng/ml of TNF-α, or 2 ng/ml of IL-1β. Equal quantities of protein from lysates of each treatment were probed by Western blotting for SOD2 (*A*) and IFIT3 (*B*). Three independent replicates were analyzed in triplicate and normalized using SOD2 (*A*) or IFIT3 (*B*) levels present in a lysate of FlagNS1 hRSV-infected A549 cells loaded in triplicate on the same membrane. Normalized integrated intensities are shown as the means ± S.E. ($n = 3$). Statistically significant difference was determined using a one-way ANOVA with Bonferroni correction. * denotes a statistical difference from mock at $p < 0.05$.

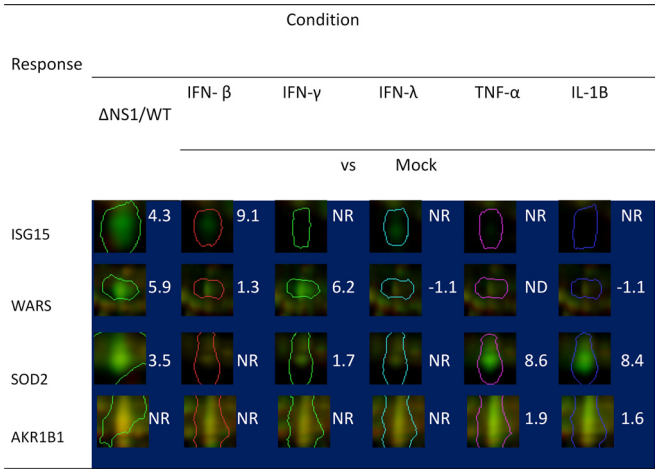

FIG. 7. **Comparisons of NS1 and cytokine regulation of selected proteins identified as being regulated in lysates of WT-GFP hRSV *versus* ΔNS1-GFP hRSV infection and cytokine stimulation of A549 cells.** Spots containing selected NS1-regulated proteins were extracted from the gel depicted in Fig. 1 for the ΔNS1/WT condition and from gels from which the impacts of treatment of A549 cells with the various cytokines were quantified by two-dimensional DIGE (Fig. 1, Table I, and supplemental Figs. 7 and 8 and supplemental Tables 3–5). WARS was identified in two regulated spots, but the intensity ratios are presented only for the most abundant isoform.

between the different infectious circumstances (Fig. 5*E*). These data indicate that NS1 does not modulate SOD2 levels in hRSV-infected A549 cells via an impact on the NRF2 pathway.

Cytokine Regulation of SOD2 Expression in A549 Cells—Various cytokines are known to induce SOD2 expression (54–59). Induction of SOD2 has only been reported in one (52) of many studies designed to assess the effect of type I IFNs. The effects of IFN-γ on SOD2 levels of A549 cells have been both positive (54, 55) and negative (56, 58, 59). Other cytokines reported to induce SOD2 expression include TNF-α and IL-1β (55–58). Thus, the potential for NS1 to influence SOD2 expression by impacting upon TNF-α, IL-1β, and IFN-dependent pathways was investigated. A549 cells were either mock treated or independently exposed to IFN-α, -β, -λ or -γ; TNF-α; or IL-1β and subsequently analyzed by Western blotting (Fig. 6). IFN-α and -β failed to cause an up-regulation of SOD2 (Fig. 6*A*) but caused substantial increases in IFIT3 (Fig. 6*B*). IFN-λ failed to exhibit induction of SOD2 (Fig. 6*A*) but caused a modest increase in IFIT3 (Fig. 6*B*) after exposure of the A549 cells for 24 h. IFN-γ caused a statistically significant induction of SOD2 (Fig. 6A) and IFIT3 (Fig. 6*B*). By comparison, TNF-α and IL-1β induced expression of SOD2 to a significant extent (Fig. 6*A*), but IFIT3 was not induced by either TNF-α or IL-1β (Fig. 6*B*). These findings indicate that modulation of SOD2 by NS1 in hRSV-infected A549 cells could potentially be via effects on IFN-γ, TNF-α, or IL-1β signaling pathways.

Quantitative Two-dimensional DIGE Analysis of Cytokine-treated A549 Cells Indicates That NS1 Suppresses Type I, II, and III IFN but Not TNF-α or IL1β Signaling Pathways—The independent biological triplicate treatments used above for Western blotting experiments were further analyzed by quantitative two-dimensional DIGE (supplemental Fig. 7 and supplemental Table 8) to compare the impacts on the proteomes of A549 cells on a more global scale. Individual protein spots seen to be differentially up-regulated by ΔNS1-GFP hRSV compared with WT-GFP hRSV infection of A549 cells (Fig. 1, Table I, and supplemental Table 4) were quantified for each of the cytokine treatments (supplemental Figs. 7 and 8). One interesting additional protein was seen to be regulated by TNF-α and IL-1β but not by any of the IFNs (supplemental Figs. 7 and 8) or by NS1. This protein was identified as aldose reductase (AKR1B1) by in-gel digestion followed by MALDI-TOF/TOF-MS/MS (supplemental Table 9). Accordingly, AKR1B1 is included in the downstream analysis of these data.

Especially informative findings from these cytokine stimulation experiments are presented pictorially by displaying sections of the two-dimensional DIGE gels containing particularly relevant protein spots for each cytokine treatment together with extracts from comparable sections of the gel comparison of WT-GFP hRSV- and ΔNS1-GFP hRSV-infected A549 cells (Fig. 7). Ratios of intensities for each of the spots are presented for each cytokine treatment relative to mock treatment and for the comparison of ΔNS1-GFP hRSV- and WT-GFP hRSV-infected A549 cell lysates. Although regulation of WARS was detected in two spots, the ratios are only pre-

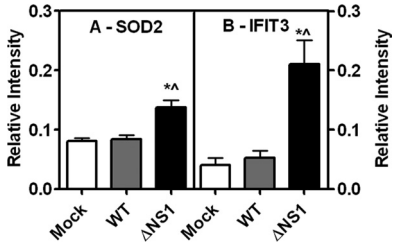

FIG. 8. **Western blot analysis of SOD2 and IFIT3 in lysates of mock infected or WT-GFP hRSV- or ΔNS1-GFP hRSV-infected Vero cells.** Equal quantities of protein from lysates of WT-GFP hRSV- or ΔNS1-GFP hRSV-infected or mock infected Vero cells were analyzed by Western blotting for SOD2 (*A*) and IFIT3 (*B*). Four independent sets of infected samples were measured with each independent set of treatments analyzed in triplicate on a separate membrane. The relative integrated intensity of each treatment was determined as a fraction to total intensity of all treatments on one membrane and then presented as the means ± S.E. ($n = 4$). Statistical analysis was performed using a one-way ANOVA for SOD2 and IFIT3 with Bonferroni correction. * and ^ denote a statistically significant difference from mock and wild-type infection, respectively, at $p < 0.05$.

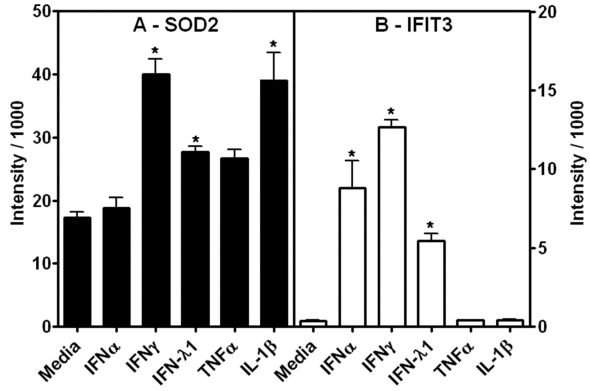

FIG. 9. **Up-regulation of SOD2 (*A*) and IFIT3 (*B*) protein expression in Vero cells by IFN-α, IFN-γ, IFN-λ1, TNF-α, and IL-1β.** Vero cells were incubated for 24 h in the presence of 6000 units/ml of IFN-α, 100 ng/ml of IFN-γ, 10 ng/ml of IFN-λ1, 20 ng/ml of TNF-α, or 1 ng/ml of IL-1β. Equal quantities of protein from lysates of each treatment were probed by Western blotting for SOD2 (*A*) and IFIT3 (*B*). Three independent replicates were analyzed in triplicate and normalized using SOD2 (*A*) or IFIT3 (*B*) levels present in a lysate of FlagNS1-infected A549 cells loaded in triplicate on the same membrane. Normalized integrated intensities are presented as the means ± S.E. ($n = 3$). Statistical significance was determined using a one-way ANOVA with Bonferroni correction. * denotes a statistical difference from mock at $p < 0.05$.

sented for the most intense of these spots. The most clear-cut outcome from this data subset relates to the NS1-regulated protein, ISG15, for which IFN-β and IFN-λ were the only cytokines tested to affect its expression. This is consistent with regulation of type I and/or type III IFN induction and/or signaling by NS1. The data for WARS also suggest an impact of NS1 on type I IFN induction and/or signaling but do not account for the level of suppression exerted by NS1. The WARS data are commensurate with an impact of NS1 on type II IFN (*i.e.* IFN-γ) activation. The data for SOD2 are compatible with the quantitative Western blot data above, which indicated that type I IFNs alone do not directly regulate this protein and that NS1 could potentially impact on induction of SOD2 expression through suppression of type II IFN, TNF-α, or IL-1β pathways. However, the level of expression of SOD2 induced by IFN-γ does not appear to be sufficient to account for the suppression of expression of this protein by NS1. Furthermore the observations made for AKR1B1 would appear to rule out an impact of NS1 on TNF-α and IL-1β pathways because expression of this protein is regulated by these two cytokines but is not affected by NS1 in infected A549 cells.

Impact of NS1 on Responses of Type I IFN-deficient Vero Cells to hRSV Infection—Vero cells are frequently used as a model type I IFN-deficient cell line for studying the role of type I IFNs in antiviral responses (60–62). Thus, Vero cells were used to investigate the possibility that although SOD2 expression is not directly induced by type I IFNs, the suppression of SOD2 expression in an infectious setting is dependent on suppressing type I IFN induction and/or signaling. To achieve this, independent triplicate sets of Vero cells were analyzed by quantitative Western blotting using SOD2- and IFIT3-specific antibodies (Fig. 8) and two-dimensional DIGE (data not shown) after infection with WT-GFP hRSV or ΔNS1-GFP hRSV or mock infection. Quantitative Western blot comparisons of mock infected and WT-GFP hRSV- and ΔNS1-GFP hRSV-infected Vero cells (Fig. 8) detected ~1.5- and 10-fold increases of SOD2 (Fig. 8*A*) and IFIT3 (Fig. 8*B*), respectively, in ΔNS1-GFP hRSV relative to mock infection but no corresponding increases of these proteins in WT-GFP hRSV-infected Vero cells (Fig. 8). In comparison, SOD2 and IFIT3 were seen to be up-regulated ~2.5- and 10-fold, respectively, in WT-GFP hRSV-infected A549 cells and 5.5- and 140-fold, respectively, in ΔNS1-GFP hRSV-infected compared with mock infected A549 cells using Western blot analysis (Fig. 4). The only statistically significant expression differences observed for SOD2 and IFIT3 by two-dimensional DIGE analyses of infected Vero cell samples was a small increase in IFIT3 in the ΔNS1-GFP hRSV-infected cell lysates (data not shown). These findings indicate that NS1 has the capacity to regulate expression of these proteins to a minor degree in a type I IFN-independent manner in Vero cells, but the major impact of NS1 on the expression of these proteins is type I IFN-dependent. In the case of SOD2, this dependence is indirect.

Cytokine stimulation of Vero cells was used to determine whether Vero cells are able to elicit different susceptibilities to those observed above for A549 cells. The major difference observed between Vero cells (Fig. 9) and A549 cells (Fig. 6) was that in Vero cells SOD2 levels exhibited a modest but statistically significant increase in response to IFN-λ1 but not TNF-α. Thus, the relatively modest NS1 regulation of SOD2 and IFIT3 expression in Vero cells may emanate from direct impacts of NS1 on type II (IFN-γ) and type III (IFN-λ) signaling. In A549 cells, NS1 would not appear to affect SOD2 levels via

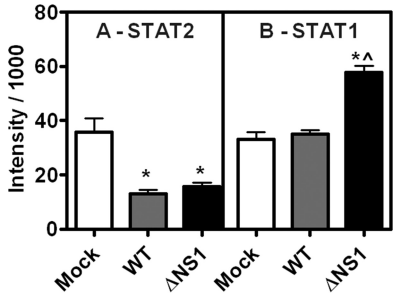

FIG. 10. **Western blot analysis of STAT2 and STAT1 in lysates of mock infected or WT-GFP hRSV- or ΔNS1-GFP hRSV-infected A549 cells.** Equal quantities of protein from lysates of WT-GFP hRSV- or ΔNS1-GFP hRSV-infected or mock infected A549 cells were analyzed by Western blotting for STAT2 (*A*) and STAT1 (*B*). The data were normalized using SOD2 or IFIT3 levels present in a lysate of FlagNS1 hRSV-infected A549 cells loaded in triplicate on the same membrane as the treatment. Normalized integrated intensities are shown as the means ± S.E. for four independent sets of treated samples measured in triplicate ($n = 4$). Statistical analysis was performed using a one-way ANOVA with Bonferroni correction. * and ^ denote a statistically significant difference from mock and wild-type infection, respectively, at $p < 0.05$.

an impact on the type III (IFN-λ) pathway (Fig. 6) but may impact directly on type II (IFN-γ) and indirectly via a type I IFN-dependent induction of SOD2 and directly on type I, type II, and type III IFN induction of IFIT3.

Analysis of the Impact of NS1 on STAT1 and STAT2 Expression during hRSV Infection of A549 Cells—STAT2 has been reported to be degraded in hRSV-infected cells (34, 35, 63) in a proteosomally mediated fashion (63). Furthermore, NS1 has been attributed with participation in STAT2 degradation (37). To assess the potential for NS1 to impact on STAT1 and STAT2 levels in response to infection, lysates of independent triplicate sets of mock infected and WT-GFP hRSV- and ΔNS1-GFP hRSV-infected A549 cells were analyzed by quantitative Western blotting using antibodies to both of these STAT proteins. STAT2 levels were significantly lower in WT-GFP hRSV-infected compared with mock infected A549 cells (Fig. 10*A*), but the levels of STAT2 were not rescued in A549 cells infected with ΔNS1-GFP hRSV (Fig. 10*A*). On the other hand, mock infected and WT-GFP hRSV-infected A549 cells had the same STAT1 levels (Fig. 10*B*), but STAT1 rose to significantly higher levels in ΔNS1-GFP hRSV-infected A549 cells. These data indicate that NS1 does not participate in STAT2 degradation in hRSV-infected cells, but it does participate in modulation of STAT1 levels.

DISCUSSION

Identification of host cell pathways regulated by viral infection and delineation of the mechanisms involved may lead to treatments for diseases caused by viruses for which development of effective vaccines and/or therapeutic agents has been elusive. Human RSV is such a virus. Transcriptional profiling of infected cells has been used to investigate the regulation of gene expression by hRSV (64–68). Proteomic approaches have the capacity to extend the insight of the impact of viral infection on cellular pathways to include potential post-transcriptional effects, as well as impacts of post-translational modifications. Comparison of the proteomes of infected and uninfected cells by two-dimensional gel electrophoresis, including in combination with two-dimensional DIGE (69, 70), has been used to detect modulation of cellular pathways by RSV (69–71). Stable isotope labeling by amino acids in cell culture in combination with one-dimensional SDS-PAGE of cellular fractions followed by LC-MS/MS of tryptic digests of gel slices has also been used to quantify changes of protein abundances in RSV-infected cells (72, 73). These studies have usually compared subcellular fractions of uninfected cells with the same cells infected with WT viruses (69–73). Regrettably, some of these studies omitted the use of biological replicates (72, 73). The present study was conducted using two-dimensional DIGE analysis of lysates of WT-GFP hRSV- and ΔNS1-GFP hRSV-infected and mock infected A549 cells that were lysed 24 h post-infection and analyzed without subcellular fractionation. This time point is several hours after the time of peak viral mRNA synthesis, which usually happens around 15 h and is at or slightly after the time of peak viral protein synthesis (2, 28) as supported by the data presented in supplemental Fig. 5*B*. Virus production starts at about 12 h and continues until the cells display extensive cytopathology at 30–48 h (supplemental Fig. 5*B*). The 24-h time point is also included in most transcriptional (63–67) and proteomic (68, 69, 71, 72) profiling studies conducted on WT hRSV-infected cells, sometimes as the unique time point for proteomic profiling (71, 72), and is the period during which A549 cells were exposed to IFN-α and/or IFN-γ prior to transcriptional profiling (47). Unfractionated lysates were used herein to avoid potential pitfalls associated with subcellular fractionation, such as selective protein losses. This lack of fractionation may have caused some low abundance regulated proteins to be obscured by dominant unregulated host cell proteins. The present study also accounted for experimental variation (*i.e.* biological and technical variation) through the use of a minimum of triplicate independent biological replicates throughout. This may also have excluded some marginally regulated proteins from observation. Collectively, the features of the present study that differentiate them from previous studies may explain the relatively small number of cellular proteins observed to be regulated by WT-GFP hRSV compared with the previous proteomic comparisons (69–73).

The truly differentiating characteristic of the present study was the use of ΔNS1-GFP hRSV infection of A549 cells. The WT hRSV genome contains NS1 and NS2, which act to tranquilize the infected cell by blocking cellular antiviral responses (16, 17, 19, 20, 25–28, 31, 32). Thus, comparing the impacts of both WT-GFP hRSV and ΔNS1-GFP hRSV on cells enabled the observation of effects that are missed in WT hRSV to mock infection comparisons and the identification of cellular

pathways that are pacified by NS1. As observed previously, this mutant virus failed to replicate as well as WT hRSV (16, 27, 28, 31), but despite this, the NS1-deficient hRSV induced a much more pronounced induction of expression of specific host cell proteins. This is consistent with biological studies that demonstrated more pronounced antiviral responses to ΔNS1 compared with WT RSVs (31, 32). The characteristics of the proteins observed to be under the regulatory influence of NS1 in the present study are also consistent with the findings of earlier biological studies that indicate that NS1 impacts in a major way on type I and type III IFN induction and signaling (31, 32, 74). However, several of the NS1-regulated proteins are also inducible by other cytokines, such as type II IFN (IFN-γ), TNF-α, and IL-1β. One NS1-regulated protein observed in the present study, SOD2, was notable in terms of lack of induction by treatment of cells with type I IFNs. A characteristic of SOD2 expression is regulation by IFN-γ (50, 54, 55), TNF-α (56–59), IL-1β (56, 57), and oxidative stress (75). SOD2 has also previously been shown to be up-regulated by RSV infection (40, 53, 66, 73). Accordingly, SOD2 was used as a probe to identify pathways that may contain molecular targets for NS1 interference, in addition to direct type I IFN induction and signaling (31, 32, 34, 36, 37).

Identification of SOD2 in the regulated protein spot evident by two-dimensional DIGE was not particularly confident from in-gel digestion protocols applied to two-dimensional gels; thus, in-solution IEF fractionation of the complete lysates was used to obtain more concentrated samples for in-gel digestion and improved identification. These fractions were further analyzed by CapHPLC-LTQ-Orbitrap-MS/MS in conjunction with spectral counting to confirm the SOD2 identification and regulation by NS1. The NS1 regulation of SOD2 was also confirmed by quantitative Western blotting. Interestingly, both the spectral counting approach and quantitative Western blotting showed some up-regulation of SOD2 in WT-GFP hRSV-infected A549 cells that was not apparent by two-dimensional DIGE analyses, which indicated a sensitivity deficiency of two-dimensional DIGE when used in the present circumstances.

Previous studies with WT hRSV-infected cells have implicated that the general oxidative stress response pathway controlled by the transcription factor NRF2 is regulated by hRSV (40, 53). Because SOD2 expression is regulated by NRF2, we probed mock infected and WT-GFP hRSV- and ΔNS1-GFP hRSV-infected A549 cell lysates with antibodies to NRF2 and two other proteins, catalase and TXNRD1, that are induced by NRF2. The data obtained from experiments conducted with two sets of independent biological triplicate samples indicated that NS1 does not impact on this pathway.

Cytokine stimulation of A549 cells in conjunction with quantitative Western blotting confirmed the lack of direct induction of SOD2 by type I IFNs and indicated that the induction of SOD2 in these cells was not due to direct type III IFN induction but was possible with IFN-γ, TNF-α, or IL-1β. Susceptibility of A549 cells to type I, type II, and type III, IFNs was indicated using IFIT3 as a marker for these pathways. IFIT3 was not seen to be regulated in A549 cells by TNF-α and IL-1β. Quantitative two-dimensional DIGE analyses of cytokine-stimulated A549 cells confirmed that NS1 does regulate type I and/or type III IFN signaling, as is evident by the fact that ISG15 was regulated by IFN-β and IFN-λ1 and that type I and type III IFN signaling does not directly induce SOD2 expression. As with the quantitative Western blotting experiments, TNF-α and IL-1β were the only cytokines capable of inducing SOD2 to levels observed in infected A549 cells, and IFN-γ had an intermediate effect. However, observations with the cellular protein, AKR1B1, indicated that NS1 does not interfere with TNF-α or IL-1β signaling because this protein was induced by both of these cytokines but was not higher in ΔNS1-GFP hRSV-infected compared with WT-GFP hRSV-infected A549 cells. Based on these observations, IFN-γ was the only cytokine signaling pathway tested that remained as a direct candidate target for NS1 interference in relation to SOD2 expression in A549 cells. A similar cross-correlation analysis was applied to regulation of the type I- and II-inducible protein, WARS. This protein was induced to a minor degree by type I IFNs but appeared to require IFN-γ induction to account for the difference in expression in ΔNS1-GFP hRSV-infected compared with WT-GFP hRSV-infected A549 cells. We have conducted other preliminary experiments involving spectral counting-based label-free relative quantification of CapHPLC-LTQ-Orbitrap-MS/MS data obtained with digests of in-solution IEF fractions of lysates of ΔNS1-GFP hRSV- and WT-GFP hRSV-infected A549 cells. Data obtained in this way identified that ICAM-1, which is induced by IFN-γ but not type I IFNs (76), is regulated by NS1. Parenthetically, it should be noted that although A549 cells are considered to be a model epithelial cell line, the ability of these cells to produce this cytokine in response to infection has been documented previously (77). As noted above, the magnitude of SOD2 induction by IFN-γ was insufficient to account for the SOD2 levels observed in WT-GFP hRSV- and ΔNS1-infected A549 cells. These findings suggest that NS1 interferes with SOD2 expression through effects on alternative or additional pathways to those assessed to date.

The potential for type I IFN signaling to contribute to the induction of SOD2 expression in infected cells was also assessed by performing the infectious experiments in Vero cells, which do not express type I IFNs (60, 61) but are capable of responding to IFN-γ (62). Interestingly, WT-GFP hRSV-infected Vero cells did not induce SOD2 as assessed by quantitative Western blot or two-dimensional DIGE (data not shown) analyses of three independent biological replicates, and only a modest statistically significant increase in SOD2 was observed in ΔNS1-GFP hRSV-infected compared with mock infected Vero cells. Similar observations were made for IFIT3. The cytokine stimulation experiments conducted with Vero cells differed from the comparable experiments con-

ducted with A549 cells in that Vero cells appeared to be responsive to type III IFN (IFN-λ) but not TNF-α in relation to both SOD2 and IFIT3 expression. Thus, the observations made with infected Vero cells could be explicable on the basis of NS1 completely interfering with both IFN-γ and IFN-λ signaling in WT-GFP hRSV-infected cells and the modest increase in expression of SOD2 and IFIT3 in ΔNS1-GFP hRSV-infected cells arising from removal of this interference. The lack of induction of SOD2 and IFIT3 in WT-GFP hRSV-infected Vero cells and the very modest induction of these proteins in ΔNS1-GFP hRSV-infected Vero cells, compared with observations made with A549 cells, imply that NS1 interferes with type I IFN signaling to impact directly on IFIT3 expression and indirectly on SOD2 expression in A549 cells.

An indirect contribution of type I IFN signaling to SOD2 induction in infected cells may be explicable based on type I IFN induction of a factor that is required to induce SOD2 (Fig. 11). The initial response of cells to paramyxovirus-negative strand viral (*e.g.* RSV) RNA and replicative intermediates involves the RNA receptor, RIG-I (78). Complexes of RIG-I and RNA are detected by a mitochondrial surface protein variously known as MAVS, IPS-1, and CARDIF (79). A cascade of responses is initiated upon activation of MAVS to induce type I IFN synthesis (Fig. 11). Resulting type I IFNs are secreted and act in a paracrine fashion to induce type I ISGs. Some of these ISGs are involved in amplification of type I IFN induction (*e.g.* RIG-I) (76). STAT1, which is required for signaling induced by types I, II, and III IFNs (80), is also an ISG product (76). Thus, type I IFN induction of STAT1 and other gene products that are ubiquitous components of all IFN signaling pathways results in amplification of all IFN responses (Fig. 11).

STAT2 is an essential component of the type I IFN signaling cascade (80). STAT2 levels have been shown to diminish in WT hRSV-infected cells via a proteosomally mediated mechanism (63), and NS1 has been attributed with forming an E3 ligase complex with Cullin2 and STAT2, resulting in polyubiquitination and proteosomal degradation of STAT2 (37). Promotion of STAT2 degradation by NS1 would attenuate production of any ISG products that may serve as indirect effectors of SOD2 induction and account for the present observations relating to the indirect type I IFN-dependent nature of SOD2 induction in hRSV-infected cells. Degradation of STAT2 would also account for attenuation of IFN-γ induction of SOD2 expression by NS1 because STAT1 is a STAT2-dependent ISG product that is obligatory for IFN-γ signaling (76, 80). The plausibility of this model is enhanced by the fact that STAT1 was observed to increase in ΔNS1-GFP hRSV-infected compared with mock infected and WT-GFP hRSV-infected cells. However, the findings that STAT2 levels diminished in WT-GFP hRSV-infected compared with mock infected cells but were not rescued upon deletion of NS1 (Ref. 35 and references therein) strongly argue against STAT2 being the target of NS1. Furthermore, other data indicate that NS2 is the main contributor to diminished STAT2 levels in RSV-infected cells (34, 35).

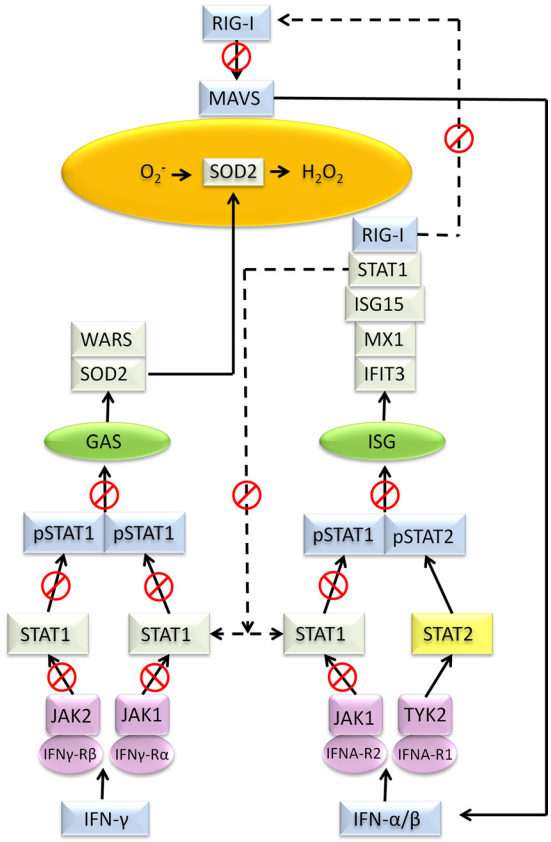

FIG. 11. **Potential modes of suppression of SOD2 expression by NS1 in hRSV infected A549 cells.** Taken together, the data obtained in this study indicate that NS1 could block SOD2 induction in hRSV-infected A549 cells by interference with pathways as marked by the *red crossed circles*. *Rectangles* indicate key proteins discussed in the text with *light green shading* indicating proteins selected from Table II as observed to be regulated by NS1, *yellow shading* indicating that STAT2 was observed but not regulated by NS1, and *light blue shading* indicating proteins not documented. *Green shaded ovals* indicate ISGs that are induced by the phospho-STAT1/phopsho-STAT2 heterodimer and IFN-γ-activated sites (*GAS*) that are induced by the phospho-STAT1 homodimer. Symbols shaded in *lavender* indicate IFN receptor subunits and their associated kinases responsible for activation of STAT1 and STAT2 by phosphorylation. The *large orange-shaded oval* represents the mitochondrion. The *solid lines* represent pathways involved in direct type I IFN induction and signaling and type II IFN signaling. The *dashed lines* represent pathways of IFN amplification initiated by type I IFN-induced gene products.

Interestingly, one of the kinases that activates STAT1, namely JAK1, is also a common component of all IFN signaling pathways (80). Thus, NS1 interference with STAT1 or JAK1 could potentially explain the present observations in terms of impact on type I, type II, and type III IFN responses (Fig. 11). However, ISG products involved in type I IFN production, hence amplification of the type I IFN response, are also potential targets. RIG-I is one such potential candidate target of NS1. It has also been shown that NS1 exhibits a

predominant mitochondrial distribution when transiently co-transfected with NS2 and during natural hRSV infection, and a role in regulation of mitochondrial pathways has been proposed (81). Of particular interest is the fact that RIG-I forms a complex that interacts with MAVS at the mitochondrial surface to induce type I IFN production (82). This interaction could potentially be involved in the induction of SOD2 expression as superoxide, which is produced in the mitochondrion (75, 82, 83) and is a known inducer of SOD2 (75). In support of this contention, it is known that reactive oxygen species are required for induction of RIG-I-mediated antiviral responses and MAVS expression (82). It is possible that deletion of NS1 from the RSV genome results in the stabilization of functional RIG-I. As a corollary, the resultant preservation of RIG-I, which is in turn amplifiable, could result in an increase in superoxide and a concomitant induction of SOD2 expression in ΔNS1-GFP hRSV-infected compared with WT-GFP hRSV-infected A549 but not Vero cells. NS1 has been implicated in regulation of members of the type I IFN induction pathway downstream of MAVS, namely TRAF3 and IKKε (36, 81). Furthermore, it is apparent that NS1 alternately regulates multiple antiviral response pathways (36) using different structural regions (36, 81). Thus, RIG-I is only one of a number of potentially plausible targets of NS1. The identity of which type I IFN gene product(s) NS1 interacts with to regulate SOD2 expression and the mechanism of this interaction remain to be determined, but the data from the current and other studies (36, 81) point to a potent impact of NS1 at the level of the mitochondrion.

The present observations also potentially account for the enhanced early apoptosis that is observed for ΔNS1 hRSV compared with WT hRSV (3, 28), which in turn supports the model that SOD2 induction in RSV-infected A549 cells is induced by superoxide. SOD2 is one of three SODs involved in reacting to oxidative stress to ameliorate downstream detrimental cellular damage (40, 83). These enzymes convert superoxide to H_2O_2, which can be a damaging oxidant if allowed to accumulate to high concentrations (40, 83). Enzymes involved in H_2O_2 metabolism to prevent downstream damage are induced by the NRF2 transcription factor, which was found not to vary in levels between mock infected and WT-GFP hRSV- and ΔNS1-GFP hRSV-infected A549 cells in the present study. Two key enzymes, catalase, which directly converts H_2O_2 to H_2O and O_2, and TXNRD1, which reduces thioredoxin and hydroperoxides (84) to ameliorate oxidative stress, were also seen not to differ between mock infected and WT-GFP hRSV- and ΔNS1 hRSV-infected A549 cells in the present study. Thus, it is feasible that increased SOD2 observed in the absence of NS1 would lead to high levels of unmetabolized H_2O_2 and enhanced apoptosis. This would be further exacerbated should the elevation of SOD2 observed with ΔNS1-GFP hRSV have arisen from elevation of superoxide (75). Precedence exists for attributing a similar imbalance of SOD2 and catalase to enhanced apoptosis of fibroblasts (83).

In summary, the proteomic comparison of WT-GFP hRSV- and ΔNS1-GFP hRSV-infected A549 cells in the present study resulted in the surprising observation that induction of SOD2 expression in response to infection was suppressed by NS1. Thus, SOD2 served as a marker for pathways that contained molecular targets for NS1 interference. Experiments involving direct cytokine stimulation of A549 and Vero cells confirmed that SOD2 expression was not directly induced by type I IFN signaling. Two-dimensional DIGE analysis of cytokine-stimulated A549 cells ruled out an impact of NS1 on TNF-α and IL-1β induction of SOD2 expression in response to infection but indicated that the IFN-γ signaling could contain molecular targets for NS1 interference. Infectious experiments with Vero cells indicated that type I IFN signaling indirectly promoted SOD2 expression in response to infection and that NS1 may target pathway components involved in amplification of the type I IFN response. Measurement of STAT1 and STAT2 in infected A549 cells excluded one contemporary hypothesis that STAT2 is a target of NS1 (37) but indicated that STAT1 is a potential target. However, other ISG products involved in amplification of the type I IFN response, such as RIG-I, could also be targets of NS1. Preliminary comparisons of WT-GFP hRSV-infected and mock infected A549 cell lysates fractionated by in-solution IEF followed by trypsin digestion and CapHPLC-LTQ-Orbitrap-MS/MS and spectral count-based quantification (not presented herein) have shown the potential to achieve a more penetrating estimate of the impact of infection of hRSV on cellular proteomes. This approach is currently being used in conjunction with ΔNS1-GFP hRSV to extend the present findings and enhance the potential to identify other pathways and molecular targets of NS1.

Acknowledgment—We gratefully acknowledge the preparation of mock and FlagNS1 hRSV-infected cell lysates for the infection time course study by Claire Straub.

* This work was supported by project grant funding from National Health and Medical Research Council Australia and the Brisbane Royal Children's Hospital Research Foundation. Preparation of infected cell lysates described in this work was funded by the NIAID, National Institutes of Health Intramural Program. Access to proteomic infrastructure funding was made possible through funds from the Australian Government National Collaborative Infrastructure Scheme provided via Bioplatforms Australia and the Queensland State Government. The costs of publication of this article were defrayed in part by the payment of page charges. This article must therefore be hereby marked "*advertisement*" in accordance with 18 U.S.C. Section 1734 solely to indicate this fact.

[S] This article contains supplemental material.

§ Present address: Yerkes National Primate Research Centre, Yerkes Genetics Laboratory, Emory University, 2409 Taylor Ln., Lawrenceville, GA 30043.

‖ Present address: Galveston National Laboratory, Center for Biodefense and Emerging Infectious Diseases, Depts. of Pathology, Microbiology & Immunology, Keiller Bldg., 301 University Blvd., University of Texas Medical Branch, Galveston, TX 77555-0609.

‡‡ To whom correspondence should be addressed: P.O. Royal Brisbane Hospital, Protein Discovery Centre, QIMR, Herston, Queen-

sland 4029 Australia. Tel.: 61-7-3845-3669; Fax: 61-7-3845-3504; E-mail: jeff.gorman@qimr.edu.au.

REFERENCES

1. Collins, P. L., Chanock, R. M., and Murphy, B. R. (2001) "Respiratory syncytial virus," in *Fields Virology* (Knipe, D. M., Howley, P. M., Griffin, D. E., Lamb, R. A., Martin, M. A., Roizman, B., and Straus, S. E., eds.) 4th Ed., pp. 1443–1485, Lippincott-Raven, Philadelphia, PA
2. Collins, P. L., and Crowe, J. E. J. (2007) "Respiratory syncytial virus and metapneumovirus," in *Fields Virology* (Knipe, D. M., Howley, P. M., Griffin, D. E., Lamb, R. A., Martin, M. A., Roizman, B., and Straus, S. E., eds.) 5th Ed., pp. 1601–1646, Lippincott-Raven, Philadelphia, PA
3. Collins, P. L., and Graham, B. S. (2008) Viral and host factors in human respiratory syncytial virus pathogenesis. *J. Virol.* **82,** 2040–2055
4. Hall, C. B. (1994) Prospects for a respiratory syncytial virus vaccine. *Science* **265,** 1393–1394
5. Levin, M. J. (1994) Treatment and prevention options for respiratory syncytial virus infections. *J. Pediatr.* **124,** S22–S27
6. Holt, P. G., and Sly, P. D. (2002) Interactions between RSV infection, asthma, and atopy: Unraveling the complexities. *J. Exp. Med.* **196,** 1271–1275
7. Sznajder, M., Stheneur, C., Albonico, V., Dib, S., Cau, D., and Chevallier, B. (2005) Respiratory development of 5- to 6- year-old children experiencing a first bronchiolitis episode before age one. *Eur. Ann. Allergy Clin. Immunol.* **37,** 392–396
8. Kapikian, A. Z., Mitchell, R. H., Chanock, R. M., Shvedoff, R. A., and Stewart, C. E. (1969) An epidemiologic study of altered clinical reactivity to respiratory syncytial (RS) virus infection in children previously vaccinated with an inactivated RS virus vaccine. *Am. J. Epidemiol.* **89,** 405–421
9. Kim, H. W., Canchola, J. G., Brandt, C. D., Pyles, G., Chanock, R. M., Jensen, K., and Parrott, R. H. (1969) Respiratory syncytial virus disease in infants despite prior administration of antigenic inactivated vaccine. *Am. J. Epidemiol.* **89,** 422–434
10. van Drunen Littel-van den Hurk, S., Mapletoft, J. W., Arsic, N., and Kovacs-Nolan, J. (2007) Immunopathology of RSV infection: Prospects for developing vaccines without this complication. *Rev. Med. Virol.* **17,** 5–34
11. Afghani, B., Ngo, T., Leu, S. Y., Wu, F. L., Cecilio, M., Aron-Johnson, P., Zeitany, R., Sills, J., and Amin, A. (2006) The effect of an interventional program on adherence to the American Academy of Pediatrics guidelines for palivizumab prophylaxis. *Pediatr. Infect. Dis. J.* **25,** 1019–1024
12. Empey, K. M., Peebles, R. S., Jr., and Kolls, J. K. Pharmacologic advances in the treatment and prevention of respiratory syncytial virus. *Clin. Infect. Dis.* **50,** 1258–1267
13. Murata, Y. (2009) Respiratory syncytial virus vaccine development. *Clin. Lab. Med.* **29,** 725–739
14. Fretzayas, A., and Moustaki, M. (2010) The challenges of RSV vaccines. Where do we stand? *Recent Pat. Antiinfect. Drug Discov.* **5,** 99–107
15. Collins, P. L., Hill, M. G., Camargo, E., Grosfeld, H., Chanock, R. M., and Murphy, B. R. (1995) Production of infectious human respiratory syncytial virus from cloned cDNA confirms an essential role for the transcription elongation factor from the 5′ proximal open reading frame of the M2 mRNA in gene expression and provides a capability for vaccine development. *Proc. Natl. Acad. Sci. U.S.A.* **92,** 11563–11567
16. Jin, H., Cheng, X., Traina-Dorge, V. L., Park, H. J., Zhou, H., Soike, K., and Kemble, G. (2003) Evaluation of recombinant respiratory syncytial virus gene deletion mutants in African green monkeys for their potential as live attenuated vaccine candidates. *Vaccine* **21,** 3647–3652
17. Jin, H., Zhou, H., Cheng, X., Tang, R., Munoz, M., and Nguyen, N. (2000) Recombinant respiratory syncytial viruses with deletions in the NS1, NS2, SH, and M2–2 genes are attenuated *in vitro* and *in vivo*. *Virology* **273,** 210–218
18. Teng, M. N., Whitehead, S. S., and Collins, P. L. (2001) Contribution of the respiratory syncytial virus G glycoprotein and its secreted and membrane-bound forms to virus replication in vitro and in vivo. *Virology* **289,** 283–296
19. Whitehead, S. S., Bukreyev, A., Teng, M. N., Firestone, C. Y., St Claire, M., Elkins, W. R., Collins, P. L., and Murphy, B. R. (1999) Recombinant respiratory syncytial virus bearing a deletion of either the NS2 or SH gene is attenuated in chimpanzees. *J. Virol.* **73,** 3438–3442
20. Munir, S., Le Nouen, C., Luongo, C., Buchholz, U. J., Collins, P. L., and Bukreyev, A. (2008) Nonstructural proteins 1 and 2 of respiratory syncytial virus suppress maturation of human dendritic cells. *J. Virol.* **82,** 8780–8796
21. Collins, P. L., and Murphy, B. R. (2005) New generation live vaccines against human respiratory syncytial virus designed by reverse genetics. *Proc. Am. Thorac. Soc.* **2,** 166–173
22. Collins, P. L., Whitehead, S. S., Bukreyev, A., Fearns, R., Teng, M. N., Juhasz, K., Chanock, R. M., and Murphy, B. R. (1999) Rational design of live-attenuated recombinant vaccine virus for human respiratory syncytial virus by reverse genetics. *Adv. Virus Res.* **54,** 423–451
23. Karron, R. A., Wright, P. F., Belshe, R. B., Thumar, B., Casey, R., Newman, F., Polack, F. P., Randolph, V. B., Deatly, A., Hackell, J., Gruber, W., Murphy, B. R., and Collins, P. L. (2005) Identification of a recombinant live attenuated respiratory syncytial virus vaccine candidate that is highly attenuated in infants. *J. Infect. Dis.* **191,** 1093–1104
24. Luongo, C., Yang, L., Winter, C. C., Spann, K. M., Murphy, B. R., Collins, P. L., and Buchholz, U. J. (2009) Codon stabilization analysis of the "248" temperature sensitive mutation for increased phenotypic stability of respiratory syncytial virus vaccine candidates. *Vaccine* **27,** 5667–5676
25. Teng, M. N., and Collins, P. L. (1999) Altered growth characteristics of recombinant respiratory syncytial viruses which do not produce NS2 protein. *J. Virol.* **73,** 466–473
26. Teng, M. N., and Collins, P. L. (2002) The central conserved cystine noose of the attachment G protein of human respiratory syncytial virus is not required for efficient viral infection *in vitro* or *in vivo*. *J. Virol.* **76,** 6164–6171
27. Teng, M. N., Whitehead, S. S., Bermingham, A., St Claire, M., Elkins, W. R., Murphy, B. R., and Collins, P. L. (2000) Recombinant respiratory syncytial virus that does not express the NS1 or M2–2 protein is highly attenuated and immunogenic in chimpanzees. *J. Virol.* **74,** 9317–9321
28. Bitko, V., Shulyayeva, O., Mazumder, B., Musiyenko, A., Ramaswamy, M., Look, D. C., and Barik, S. (2007) Nonstructural proteins of respiratory syncytial virus suppress premature apoptosis by an NF-κB-dependent, interferon-independent mechanism and facilitate virus growth. *J. Virol.* **81,** 1786–1795
29. Kotelkin, A., Belyakov, I. M., Yang, L., Berzofsky, J. A., Collins, P. L., and Bukreyev, A. (2006) The NS2 protein of human respiratory syncytial virus suppresses the cytotoxic T-cell response as a consequence of suppressing the type I interferon response. *J. Virol.* **80,** 5958–5967
30. Moore, E. C., Barber, J., and Tripp, R. A. (2008) Respiratory syncytial virus (RSV) attachment and nonstructural proteins modify the type I interferon response associated with suppressor of cytokine signaling (SOCS) proteins and IFN-stimulated gene-15 (ISG15). *Virol. J.* **5,** 116
31. Spann, K. M., Tran, K. C., Chi, B., Rabin, R. L., and Collins, P. L. (2004) Suppression of the induction of α, β, and λ interferons by the NS1 and NS2 proteins of human respiratory syncytial virus in human epithelial cells and macrophages [corrected]. *J. Virol.* **78,** 4363–4369
32. Spann, K. M., Tran, K. C., and Collins, P. L. (2005) Effects of nonstructural proteins NS1 and NS2 of human respiratory syncytial virus on interferon regulatory factor 3, NF-κB, and proinflammatory cytokines. *J. Virol.* **79,** 5353–5362
33. Ling, Z., Tran, K. C., and Teng, M. N. (2009) Human respiratory syncytial virus nonstructural protein NS2 antagonizes the activation of β interferon transcription by interacting with RIG-I. J. *Virol.* **83,** 3734–3742
34. Lo, M. S., Brazas, R. M., and Holtzman, M. J. (2005) Respiratory syncytial virus nonstructural proteins NS1 and NS2 mediate inhibition of Stat2 expression and α/β interferon responsiveness. *J. Virol.* **79,** 9315–9319
35. Ramaswamy, M., Shi, L., Varga, S. M., Barik, S., Behlke, M. A., and Look, D. C. (2006) Respiratory syncytial virus nonstructural protein 2 specifically inhibits type I interferon signal transduction. *Virology* **344,** 328–339
36. Swedan, S., Musiyenko, A., and Barik, S. (2009) Respiratory syncytial virus nonstructural proteins decrease levels of multiple members of the cellular interferon pathways. *J. Virol.* **83,** 9682–9693
37. Elliott, J., Lynch, O. T., Suessmuth, Y., Qian, P., Boyd, C. R., Burrows, J. F., Buick, R., Stevenson, N. J., Touzelet, O., Gadina, M., Power, U. F., and Johnston, J. A. (2007) Respiratory syncytial virus NS1 protein degrades STAT2 by using the Elongin-Cullin E3 ligase. *J. Virol.* **81,** 3428–3436
38. Chambers, R., and Takimoto, T. (2009) Host specificity of the anti-interferon and anti-apoptosis activities of parainfluenza virus P/C gene products. *J. Gen. Virol.* **90,** 1906–1915
39. Huang, Y. T., Collins, P. L., and Wertz, G. W. (1985) Characterization of the

10 proteins of human respiratory syncytial virus: Identification of a fourth envelope-associated protein. *Virus Res.* **2,** 157–173
40. Hosakote, Y. M., Liu, T., Castro, S. M., Garofalo, R. P., and Casola, A. (2009) Respiratory syncytial virus induces oxidative stress by modulating antioxidant enzymes. *Am. J. Respir. Cell Mol. Biol.* **41,** 348–357
41. Kotenko, S. V., Gallagher, G., Baurin, V. V., Lewis-Antes, A., Shen, M., Shah, N. K., Langer, J. A., Sheikh, F., Dickensheets, H., and Donnelly, R. P. (2003) IFN-λs mediate antiviral protection through a distinct class II cytokine receptor complex. *Nat. Immunol.* **4,** 69–77
42. Laemmli, U. K. (1970) Cleavage of structural proteins during the assembly of the head of bacteriophage T4. *Nature* **227,** 680–685
43. Candiano, G., Bruschi, M., Musante, L., Santucci, L., Ghiggeri, G. M., Carnemolla, B., Orecchia, P., Zardi, L., and Righetti, P. G. (2004) Blue silver: A very sensitive colloidal Coomassie G-250 staining for proteome analysis. *Electrophoresis* **25,** 1327–1333
44. Dave, K. A., Hamilton, B. R., Wallis, T. P., Furness, S. G. B., Whitelaw, M. L., and Gorman, J. J. (2007) Identification of N,N^{ε}-dimethyl-lysine in the murine dioxin receptor using MALDI-TOF/TOF- and ESI-LTQ-Orbitrap-FT-MS. *Int. J. Mass Spectrom.* **268,** 168–180
45. Dave, K. A., Headlam, M. J., Wallis, T. P., and Gorman, J. J. (2011) Preparation and analysis of proteins and peptides using MALDI TOF/TOF mass spectrometry. Current Protocols in Protein Science **63,** 16.13.1–16.13.21.
46. Erdjument-Bromage, H., Lui, M., Lacomis, L., Grewal, A., Annan, R. S., McNulty, D. E., Carr, S. A., and Tempst, P. (1998) Examination of micro-tip reversed-phase liquid chromatographic extraction of peptide pools for mass spectrometric analysis. *J. Chromatogr. A* **826,** 167–181
47. Aldridge, G. M., Podrebarac, D. M., Greenough, W. T., and Weiler, I. J. (2008) The use of total protein stains as loading controls: An alternative to high-abundance single-protein controls in semi-quantitative immunoblotting. *J. Neurosci. Methods* **172,** 250–254
48. Livak, K. J., and Schmittgen, T. D. (2001) Analysis of relative gene expression data using real-time quantitative PCR and the $2^{-\Delta\Delta C_T}$ method. *Methods* **25,** 402–408
49. Smith, B. T. (1977) Cell line A549: A model system for the study of alveolar type II cell function. *Am. Rev. Respir. Dis.* **115,** 285–293
50. Sanda, C., Weitzel, P., Tsukahara, T., Schaley, J., Edenberg, H. J., Stephens, M. A., McClintick, J. N., Blatt, L. M., Li, L., Brodsky, L., and Taylor, M. W. (2006) Differential gene induction by type I and type II interferons and their combination. *J. Interferon Cytokine Res.* **26,** 462–472
51. Schlender, J., Bossert, B., Buchholz, U., and Conzelmann, K. K. (2000) Bovine respiratory syncytial virus nonstructural proteins NS1 and NS2 cooperatively antagonize α/β interferon-induced antiviral response. *J. Virol.* **74,** 8234–8242
52. Lu, G., Shimizu, I., Cui, X., Itonaga, M., Tamaki, K., Fukuno, H., Inoue, H., Honda, H., and Ito, S. (2002) Interferon-α enhances biological defense activities against oxidative stress in cultured rat hepatocytes and hepatic stellate cells. *J. Med. Invest.* **49,** 172–181
53. Cho, H. Y., Imani, F., Miller-DeGraff, L., Walters, D., Melendi, G. A., Yamamoto, M., Polack, F. P., and Kleeberger, S. R. (2009) Antiviral activity of NRF2 in a murine model of respiratory syncytial virus disease. *Am. J. Respir. Crit Care Med.* **179,** 138–150
54. Harris, C. A., Derbin, K. S., Hunte-McDonough, B., Krauss, M. R., Chen, K. T., Smith, D. M., and Epstein, L. B. (1991) Manganese superoxide dismutase is induced by IFN-γ in multiple cell types: Synergistic induction by IFN-γ and tumor necrosis factor or IL-1. *J. Immunol.* **147,** 149–154
55. Chung-man Ho, J., Zheng, S., Comhair, S. A., Farver, C., and Erzurum, S. C. (2001) Differential expression of manganese superoxide dismutase and catalase in lung cancer. *Cancer Res.* **61,** 8578–8585
56. Wong, G. H., and Goeddel, D. V. (1988) Induction of manganous superoxide dismutase by tumor necrosis factor: Possible protective mechanism. *Science* **242,** 941–944
57. Rogers, R. J., Monnier, J. M., and Nick, H. S. (2001) Tumor necrosis factor-α selectively induces MnSOD expression via mitochondria-to-nucleus signaling, whereas interleukin-1β utilizes an alternative pathway. *J. Biol. Chem.* **276,** 20419–20427
58. Warner, B. B., Burhans, M. S., Clark, J. C., and Wispé, J. R. (1991) Tumor necrosis factor-α increases Mn-SOD expression: Protection against oxidant injury. *Am. J. Physiol.* **260,** L296–L301
59. Sana, T. R., Janatpour, M. J., Sathe, M., McEvoy, L. M., and McClanahan, T. K. (2005) Microarray analysis of primary endothelial cells challenged with different inflammatory and immune cytokines. *Cytokine* **29,** 256–269
60. Desmyter, J., Melnick, J. L., and Rawls, W. E. (1968) Defectiveness of interferon production and of rubella virus interference in a line of African green monkey kidney cells (Vero). *J. Virol.* **2,** 955–961
61. Emeny, J. M., and Morgan, M. J. (1979) Regulation of the interferon system: Evidence that Vero cells have a genetic defect in interferon production. *J. Gen. Virol.* **43,** 247–252
62. Wathelet, M. G., Berr, P. M., and Huez, G. A. (1992) Regulation of gene expression by cytokines and virus in human cells lacking the type-I interferon locus. *Eur. J. Biochem.* **206,** 901–910
63. Ramaswamy, M., Shi, L., Monick, M. M., Hunninghake, G. W., and Look, D. C. (2004) Specific inhibition of type I interferon signal transduction by respiratory syncytial virus. *Am. J. Respir. Cell Mol. Biol.* **30,** 893–900
64. Janssen, R., Pennings, J., Hodemaekers, H., Buisman, A., van Oosten, M., de Rond, L., Oztürk, K., Dormans, J., Kimman, T., and Hoebee, B. (2007) Host transcription profiles upon primary respiratory syncytial virus infection. *J. Virol.* **81,** 5958–5967
65. Martínez, I., Lombardía, L., García-Barreno, B., Domínguez, O., and Melero, J. A. (2007) Distinct gene subsets are induced at different time points after human respiratory syncytial virus infection of A549 cells. *J. Gen. Virol.* **88,** 570–581
66. Mayer, A. K., Muehmer, M., Mages, J., Gueinzius, K., Hess, C., Heeg, K., Bals, R., Lang, R., and Dalpke, A. H. (2007) Differential recognition of TLR-dependent microbial ligands in human bronchial epithelial cells. *J. Immunol.* **178,** 3134–3142
67. Tian, B., Zhang, Y., Luxon, B. A., Garofalo, R. P., Casola, A., Sinha, M., and Brasier, A. R. (2002) Identification of NF-κB-dependent gene networks in respiratory syncytial virus-infected cells. *J. Virol.* **76,** 6800–6814
68. Zhang, Y., Luxon, B. A., Casola, A., Garofalo, R. P., Jamaluddin, M., and Brasier, A. R. (2001) Expression of respiratory syncytial virus-induced chemokine gene networks in lower airway epithelial cells revealed by cDNA microarrays. *J. Virol.* **75,** 9044–9058
69. Jamaluddin, M., Wiktorowicz, J. E., Soman, K. V., Boldogh, I., Forbus, J. D., Spratt, H., Garofalo, R. P., and Brasier, A. R. (2010) Role of peroxiredoxin 1 and peroxiredoxin 4 in protection of respiratory syncytial virus-induced cysteinyl oxidation of nuclear cytoskeletal proteins. *J. Virol.* **84,** 9533–9545
70. van Diepen, A., Brand, H. K., Sama, I., Lambooy, L. H., van den Heuvel, L. P., van der Well, L., Huynen, M., Osterhaus, A. D., Andeweg, A. C., and Hermans, P. W. (2010) Quantitative proteome profiling of respiratory virus-infected lung epithelial cells. *J. Proteomics* **73,** 1680–1693
71. Brasier, A. R., Spratt, H., Wu, Z., Boldogh, I., Zhang, Y., Garofalo, R. P., Casola, A., Pashmi, J., Haag, A., Luxon, B., and Kurosky, A. (2004) Nuclear heat shock response and novel nuclear domain 10 reorganization in respiratory syncytial virus-infected A549 cells identified by high-resolution two-dimensional gel electrophoresis. *J. Virol.* **78,** 11461–11476
72. Munday, D. C., Emmott, E., Surtees, R., Lardeau, C. H., Wu, W., Duprex, W. P., Dove, B. K., Barr, J. N., and Hiscox, J. A. (2010) Quantitative proteomic analysis of A549 cells infected with human respiratory syncytial virus. *Mol. Cell. Proteomics* **9,** 2438–2459
73. Munday, D. C., Hiscox, J. A., and Barr, J. N. (2010) Quantitative proteomic analysis of A549 cells infected with human respiratory syncytial virus subgroup B using SILAC coupled to LC-MS/MS. *Proteomics* **10,** 4320–4334
74. Bossert, B., Marozin, S., and Conzelmann, K. K. (2003) Nonstructural proteins NS1 and NS2 of bovine respiratory syncytial virus block activation of interferon regulatory factor 3. *J. Virol.* **77,** 8661–8668
75. Hu, Y., Rosen, D. G., Zhou, Y., Feng, L., Yang, G., Liu, J., and Huang, P. (2005) Mitochondrial manganese-superoxide dismutase expression in ovarian cancer: Role in cell proliferation and response to oxidative stress. *J. Biol. Chem.* **280,** 39485–39492
76. Der, S. D., Zhou, A., Williams, B. R., and Silverman, R. H. (1998) Identification of genes differentially regulated by interferon α, β, or γ using oligonucleotide arrays. *Proc. Natl. Acad. Sci. U.S.A.* **95,** 15623–15628
77. Sharma, M., Sharma, S., Roy, S., Varma, S., and Bose, M. (2007) Pulmonary epithelial cells are a source of interferon-gamma in response to *Mycobacterium tuberculosis* infection. *Immunol. Cell Biol.* **85,** 229–237
78. Nakhaei, P., Genin, P., Civas, A., and Hiscott, J. (2009) RIG-I-like receptors: Sensing and responding to RNA virus infection. *Semin. Immunol.* **21,** 215–222

79. Scott, I. (2009) Mitochondrial factors in the regulation of innate immunity. *Microbes Infect.* **11,** 729–736
80. Sadler, A. J., and Williams, B. R. (2008) Interferon-inducible antiviral effectors. *Nat. Rev. Immunol.* **8,** 559–568
81. Swedan, S., Andrews, J., Majumdar, T., Musiyenko, A., and Barik, S. (2011) Multiple functional domains and complexes of the two nonstructural proteins of human respiratory syncytial virus contribute to interferon suppression and cellular location. *J. Virol.* **85,** 10090–10100
82. Soucy-Faulkner, A., Mukawera, E., Fink, K., Martel, A., Jouan, L., Nzengue, Y., Lamarre, D., Vande Velde, C., and Grandvaux, N. (2010) Requirement of NOX2 and reactive oxygen species for efficient RIG-I-mediated antiviral response through regulation of MAVS expression. *PLoS Pathog.* **6,** e1000930
83. Hussain, S. P., Amstad, P., He, P., Robles, A., Lupold, S., Kaneko, I., Ichimiya, M., Sengupta, S., Mechanic, L., Okamura, S., Hofseth, L. J., Moake, M., Nagashima, M., Forrester, K. S., and Harris, C. C. (2004) p53-induced up-regulation of MnSOD and GPx but not catalase increases oxidative stress and apoptosis. *Cancer Res.* **64,** 2350–2356
84. Mustacich, D., and Powis, G. (2000) Thioredoxin reductase. *Biochem. J.* **346,** 1–8